Cell shape change and invagination of the cephalic furrow involves reorganization of F-actin

Allison K. Spencer, Bilal A. Siddiqui [1], Jeffrey H. Thomas *

Department of Cell Biology and Biochemistry, Texas Tech University Health Sciences Center, 3601 4th Street, STOP 6540, Lubbock, TX 79430, United States

A B S T R A C T

Invagination of epithelial sheets to form furrows is a fundamental morphogenetic movement and is found in a variety of developmental events including gastrulation and vertebrate neural tube formation. The cephalic furrow is a deep epithelial invagination that forms during Drosophila gastrulation. In the first phase of cephalic furrow formation, the initiator cells that will lead invagination undergo apicobasal shortening and apical constriction in the absence of epithelial invagination. In the second phase of cephalic furrow formation, the epithelium starts to invaginate, accompanied by both basal expansion and continued apicobasal shortening of the initiator cells. The cells adjacent to the initiator cells also adopt wedge shapes, but only after invagination is well underway. Myosin II does not appear to drive apical constriction in cephalic furrow formation. However, cortical F-actin is increased in the apices of the initiator cells and in invaginating cells during both phases of cephalic furrow formation. These findings suggest that a novel mechanism for epithelial invagination is involved in cephalic furrow formation.

© 2015 Elsevier Inc. All rights reserved.

Introduction

One of the fundamental morphogenetic processes that shape the embryo during development is the invagination, or inward bending, of epithelial sheets (Davidson et al., 1995; Ettensohn, 1985; Fristrom, 1988; Keller et al., 2003; Lecuit and Lenne, 2007; Martin and Goldstein, 2014; Odell et al., 1981; Sawyer et al., 2010). Differences in cell shape changes and movements can produce a variety of epithelial structures (Davidson, 2012; Quintin et al., 2008). Despite the variety of epithelial structures ultimately produced, in the best-studied epithelial invaginations, invagination is associated with apical constriction (Sawyer et al., 2010). Actomyosin contraction appears to be the predominant mechanism of apical constriction and epithelial invagination (Martin and Goldstein, 2014; Sawyer et al., 2010; Sherrard et al., 2010). However, theoretical and modeling studies suggest other possible mechanisms of epithelial invagination, as have experimental studies (Davidson et al., 1995, 1999; Ettensohn, 1985; Fristrom, 1988; Herman et al., 1999; Keller et al., 2003; Kondo and Hayashi, 2013; Wang et al., 2012).

The cephalic furrow (CF) starts to form at the beginning of gastrulation (stage 6), when the ventral furrow starts to form. The CF first appears as a shallow groove at about 65% egg length (EL, measured from the posterior of the embryo) on the lateral sides of the embryo. The groove extends both postero-dorsally and antero-ventrally, eventually forming a ring around the entire embryo. The ring becomes more canted such that by the end of stage 7, the CF ring extends from 54% EL dorsally to 74% EL ventrally (Campos-Ortega and Hartenstein, 1997; Turner and Mahowald, 1977). As gastrulation progresses, the CF rapidly grows deeper. By stage 8, it becomes very deep on the lateral sides, but the ventral and dorsal regions remain relatively shallow (Campos-Ortega and Hartenstein, 1997; Costa et al., 1993; Underwood et al., 1980). Starting during stage 8, several cell divisions occur in the invaginated furrow and might contribute to further CF deepening (Campos-Ortega and Hartenstein, 1997; Foe, 1989). The CF is transient and by stage 11, after germband extension has completed but before germband retraction begins, the CF has unfolded and all the cells that had invaginated have returned to the surface (Campos-Ortega and Hartenstein, 1997; Costa et al., 1993; Turner and Mahowald, 1977).

Little is known about the cell shape changes that occur during CF formation. CF formation is initiated by the shortening of a row of cells in the mid-lateral region of the embryo. These initiator cells undergo a cell shape change from columnar cells to bottle-shaped cells that includes apical constriction, shortening in the apicobasal axis and shifting of the nuclei to a more basal position during the beginning of CF formation (Costa et al., 1993; Turner and Mahowald, 1977; Vincent et al., 1997). However, the apices of the CF initiator cells narrow less than those of the ventral furrow (Costa et al., 1993). Unlike the cells of the ventral furrow, they do not undergo apical flattening or ruffling (Costa et al., 1993; Turner

---

* Corresponding author.
   E-mail address: jeffrey.thomas@ttuhsc.edu (J.H. Thomas).
   [1] Current address: Yale School of Medicine, 333 Cedar Street, New Haven, CT 06510, United States.
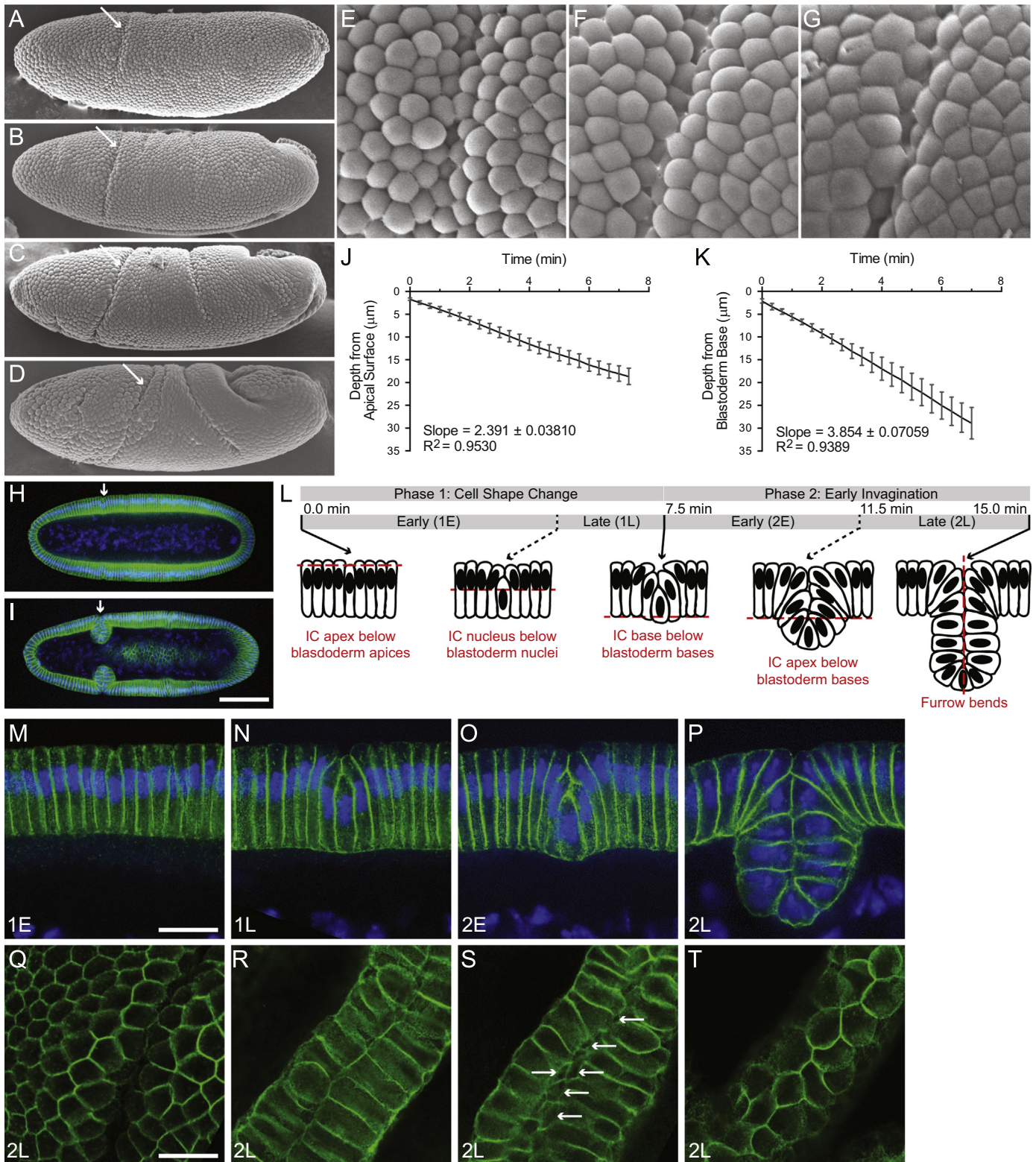
Fig. 1. Morphogenesis of the early cephalic furrow. (A–G) Scanning electron micrographs of gastrulating embryos showing the lateral surface (A–D) and corresponding surface cells in and near the CF (E–G) at early stage 6 (A,E), late stage 6 (B,F), stage 7 (C,G) and stage 8 (D). Arrow: cephalic furrow (CF). (H–I) Confocal images of gastrulating embryos showing cell membranes (Nrt, green) and nuclei (Hoechst, blue) at stage 6 (H) and stage 7 (I). Arrow: CF. Scale bar: 100 μm. (J) Time course analysis of the depth of the CF cleft measured from the apical blastoderm surface. Mean and SD. (K) Later time course analysis of the depth of CF invagination into the yolk sac measured from the blastoderm base. Time point 0 was approximately 7.5 min after time point 0 in (J). Mean and SD. (L) Key morphological features defining the two phases of early CF formation and timeline. (M–P) Confocal images of CF formation in the lateral region of the gastrulating embryo showing cells at early phase 1 (1E) (M), late phase 1 (1L) (N), early phase 2 (2E) (O) and late phase 2 (2L) (P). Scale bar: 20 μm. (Q–T) Confocal sagittal images of CF formation from z-stacks of two different embryos at late phase 2 showing cells at the surface of furrow cleft (Q), internalized cells of the CF (R), initiator cell apices (arrows) (S), and basal regions of initiator cells near the base of the CF (T). Scale bar: 20 μm. Anterior: left.

and Mahowald, 1977). As the furrow cleft deepens, the apices of the neighboring cells appear to 'roll over' into the cleft (Costa et al., 1993; Vincent et al., 1997).

The CF is not associated with any particular cell fate (Campos-Ortega and Hartenstein, 1997; Underwood et al., 1980). However, CF formation is regulated by the anteroposterior and dorsoventral axial patterning systems. The second row of cells expressing *even-skipped* (*eve*) in *eve* stripe 1 become the initiator cells (Harding et al., 1986; Vincent et al., 1997). The identity of the initiator cells is specified by the anteroposterior patterning genes *bicoid* (*bcd*), *hunchback* (*hb*), *buttonhead* (*btd*), *paired* (*prd*) and *eve* (Blankenship and Wieschaus, 2001; Driever and Nusslein-Volhard, 1988; Frohnhofer and Nusslein-Volhard, 1986; Lehmann and Nusslein-Volhard, 1987; Namba et al., 1997; Payre et al., 1994; Schupbach and Wieschaus, 1986, 1989; Struhl et al., 1989; Vincent et al., 1997). Dorsoventral differences in CF depth depend on the dorsoventral patterning genes (Anderson et al., 1985; Costa et al., 1993; Irish and Gelbart, 1987; Roth et al., 1991; Rushlow and Levine, 1990; Zusman et al., 1988; Zusman and Wieschaus, 1985).

Here, we characterize CF formation at the morphological and cellular levels. We observed that cell shape changes during CF invagination differed from those described for other epithelial invaginations that occur during gastrulation. Furthermore, we observed that actin, adherens junctions and myosin II are reorganized during CF formation. Myosin II appeared to be reorganized in response to apical constriction. We propose that apicobasal shortening and basal expansion drive CF formation rather than actomyosin-mediated apical constriction.

Results

Cephalic furrow formation

CF formation starts near the beginning of gastrulation on the lateral side of the embryo at early stage 6 as a shallow indentation of a single row of cells (Fig. 1A). As gastrulation progresses, the CF extends circumferentially and becomes a deep, prominent infolding of the epithelial blastoderm (Fig. 1B–D). Observation of the surface morphology of the early CF by scanning electron microscopy (SEM) revealed that at the beginning of CF formation, initiator cell apices dropping below the surface remained dome-shaped like their immediate and more distal neighbors (Fig. 1A and E). During late stage 6, the apices of the immediate neighbors of the initiator cells, the adjacent cells, remained dome-shaped as they bent inwards towards the forming CF cleft (Fig. 1B and F). By stage 7, all cell apices had a shallower dome-shape, including the apices of the cells entering the CF cleft (Fig. 1C and G).

To visualize internal CF morphology at the deepest part of CF invagination, we imaged gastrulae in the plane midway between the dorsal and ventral sides. During early gastrulation, the initiator cells underwent cell shape changes without bending the epithelium or moving into the interior (Fig. 1H). Later during gastrulation, the initiator cells formed the hinge point of an epithelial fold that invaginates into the yolk sac (Fig. 1I). The apices of the infolded cells were closely apposed (Fig. 1I). As morphogenesis proceeded, the CF turned anteriorly as more cells invaginated and the CF deepened. Here, we focus on the morphogenesis of the CF before turning (Fig. 1H and I), when cell shape changes and movements are simple and more easily visualized.

Using time-lapse microscopy, we measured two major morphological changes: the depth of invagination from the surface at the beginning of CF formation and the depth of the fold's invagination into the interior of the embryo later during CF formation. These occurred at different times. During the first 7 min of CF formation, the initiator cell apices invaginated about 18 μm from

the surface, at about 2.4 μm/min (Fig. 1J). This was the first phase of CF formation. In the second phase of CF formation, the epithelium invaginated. The depth of CF movement into the yolk sac was measured starting from the initial distinctive bulge of the initiator cell bases into the yolk sac, about 7.5 min after invagination from the surface began. Over the next 7 min, the epithelial fold invaginated about 29 μm from the blastoderm base, at about 3.9 μm/min (Fig. 1K).

Phase 1, the initial cell shape change phase, begins within 2 min, before or after, completion of cellularization. The beginning is marked by the dropping of the apices of the initiator cells below the apices of the other cells of the cellular blastoderm. Phase 1 consists of apicobasal shortening of the initiator cells, basal movement of the initiator cell nuclei, and constriction of initiator cell apices. The cells adjacent to the initiator cells bend inward (Fig. 1L–N). For ease of presentation, we divided phase 1 into early and late parts based on the position of the initiator cell nuclei. By late phase 1, the bases of the initiator cells and adjacent cells have started to bulge slightly into the yolk sac (Fig. 1N). During phase 2, the invagination phase, the bases of the initiator cells start to invaginate into the yolk sac. The initiator cells continue to undergo apicobasal shortening and become increasingly wedge-shaped (Fig. 1L,O and P). We have also divided phase 2 into early and late parts based on the position of the initiator cells. Phase 2 ends when the CF has reached its maximum depth perpendicular to the non-invaginated cellular blastoderm before turning anteriorly (Fig. 1L).

Time-lapse imaging of initiator cells was conducted by simultaneous two-channel confocal imaging of embryos expressing both Spider-GFP and H2A-RFP (Fig. 2A, Supplemental Movie 1). Basal movement of the initiator cell nucleus started within 1.5 min, before or after, the start of initiator cell apex invagination (Fig. 2B). *en-face* time-lapse imaging of the subapical region of initiator cells during phase 1E showed that the initiator cell apices constricted perpendicular to the forming CF cleft, but not along the cleft (Fig. 2C, Supplemental Movie 2).

Cells moving into the CF had apices that extended towards the edge of the furrow cleft (Fig. 1O–Q). By late phase 2, cells that had been internalized into the epithelial fold were shorter and their apices were closely apposed (Fig. 1P and R). The initiator cells had dramatically altered shape, having become very short and wedge-shaped (Fig. 1P,S and T). The initiator cell apices were anisotropic: apical width was unaltered in the plane of the CF fold, but reduced in the perpendicular plane (Fig. 1S). This geometry allowed formation of an epithelial fold with closely apposed apices. The bases of the initiator cells were roughly isotropic (Fig. 1T).

Cell shape changes during early cephalic furrow morphogenesis

We quantitatively analyzed cell shape change during early CF formation by measuring the initiator cells, the cells adjacent to the initiator cells, cells that had not invaginated into the CF, cells at the edge of the furrow cleft, and cells that had invaginated into the epithelial fold (Fig. 3A).

Cells that have not invaginated into the cephalic furrow

At the start of gastrulation, the cells of the cellular blastoderm were columnar epithelial cells of approximately the same size. The majority of cells that had not invaginated were between 30 and 36 μm in height throughout most of early CF formation, but somewhat shorter (26–30 μm) during late phase 2 (Fig. 3B). Nuclei in non-invaginated cells remained at the same position, about 62% of cell height, during early CF formation (Fig. 3C). The widths of the apices and bases of non-invaginated cells were about 5–6 μm, and remained unchanged throughout early CF formation (Fig. 3D
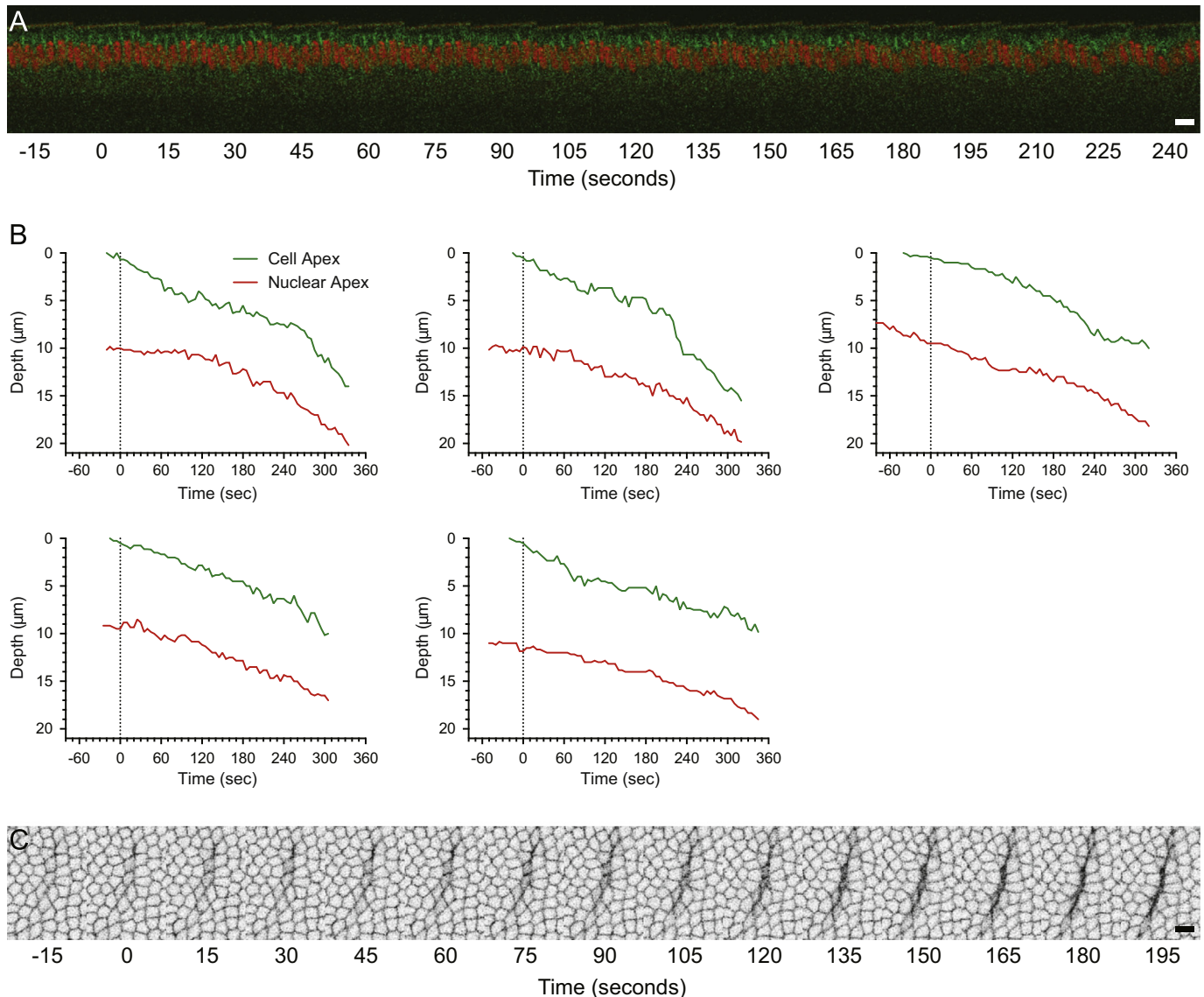
Fig. 2. Initiator cell dynamics during early cephalic furrow formation. (A) Time-lapse montage showing cell membranes (Spider-GFP, green) and nuclei (H2A-mRFP, red) of the CF region during early phase 1 (from Supplemental Movie 1). (B) Graphs showing change in initiator cell apex depth from surface and initiator cell nuclear apex depth during part of phase 1 in individual embryos. Graph 2 is from data shown in montage (A). Time point zero was defined as the first 5 s. interval that the initiator cell apex was at least 0.5 µm below the surface (A–B). (C) Inverted *en-face* time-lapse montage showing subapical cell membranes (Spider-GFP) of the lateral CF region (from Supplemental Movie 2). Scale bars: 10 µm.

and E). Non-invaginated cells remained columnar throughout early CF formation: the aspect ratios (width:height) were about 0.2 (Fig. 4B).

Initiator cells

During CF formation, the initiator cells underwent the first and most extensive cell shape changes. Initiator cells shortened dramatically throughout CF formation, such that they were typically half the height of non-invaginated cells by late phase 2 (Fig. 3B). Nuclei moved basally: initiator cells had a median relative nuclear position of 0.55 in early phase 1 and 0.42 in late phase 2, whereas non-invaginated cells had a median relative nuclear position of 0.62 (Fig. 3C).

Initiator cells adopted a wedge-like shape during CF formation. The degree to which a cell was wedge-shaped was described quantitatively as the ratio between apical and basal widths of the cell. In typical columnar epithelial cells, such as non-invaginated cells, this ratio was 1.0 (Fig. 3D). In early phase 1, the median apical to basal width ratio was 0.39 (Fig. 3D), indicating an early
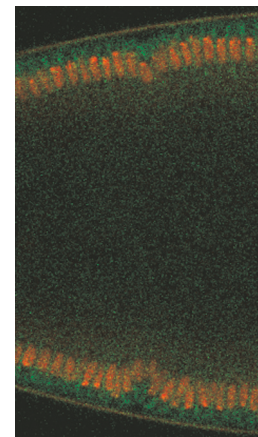
Movie 1. Confocal time-lapse images of Spider-GFP (green, membrane) and H2A-RFP (red, nuclei) during early CF formation. A video clip is available online.Supplementary material related to this article can be found online at http://dx.doi.org/10.1016/j.ydbio.2015.03.022.

beginning of the columnar to wedge cell shape transition. This ratio declined to a median of 0.07 in late phase 2 as the wedge shape became more pronounced (Fig. 3D). Initiator cell wedging involved both apical constriction and basal expansion. Apical constriction occurred in early phase 1 (Fig. 3E). Basal expansion had a very different dynamic. No basal expansion occurred in early phase 1: the bases of initiator cells and non-invaginated cells were the same width (Fig. 3E). Basal expansion occurred during phase 2 (Fig. 3E). Throughout all stages of early CF formation, the initiator cell apical aspect ratio (ratio of apical width to height) had a median of about 0.05 and remained roughly constant despite cell shortening (Fig. 4B). However, the initiator cell basal aspect ratio

(ratio of basal width to height) increased during early CF formation. During phase 1, the basal aspect ratio was indistinguishable from the non-invaginated cell basal aspect ratio, but increased during phase 2. By late phase 2, the median basal aspect ratio of
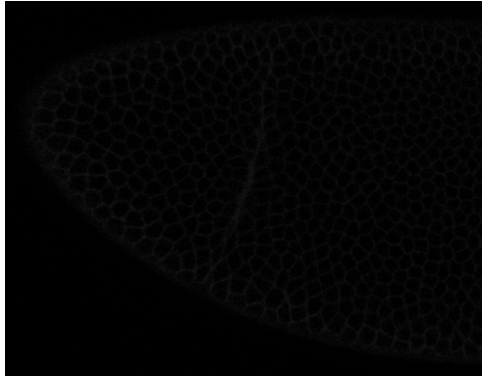
Movie 2. Confocal *en-face* time-lapse images of Spider-GFP during early CF formation. A video clip is available online.Supplementary material related to this article can be found online at http://dx.doi.org/10.1016/j.ydbio.2015.03.022.

Fig. 3. Morphometric analysis of cell shape changes during early cephalic furrow formation. (A) Diagram of early CF formation showing morphological classes of cells during phase 1 and phase 2. Initiator cells, cells making the initial cell shape changes during CF formation (IC, green); adjacent cells, cells immediately anterior and posterior to the initiator cells (Adj, blue); cells that have not folded into the CF (Non, gray); cells that have moved into the CF (Inv, red); cells at the edge of the CF cleft (Edg, brown). (B) Cell heights. IC became shorter at every stage ($p < 0.01$); Adj did not change during phase 1, but became shorter between phase 1 and phase 2 ($p < 0.0001$). Non became shorter during phase 2L ($p < 0.0001$). During phase 1E, IC was shorter than Adj ($p < 0.01$) and Non ($p < 0,0001$); Adj and Non did not differ. All cell classes differed during phase 1L ($p < 0.0001$) and 2E ($p < 0.001$). IC and Adj did not differ in height during phase 2L, but all other cell classes did ($p < 0.0001$). (C) Relative position of nuclei to cell height. Nuclear position differed in IC between phase 1E and 2 ($p < 0.001$), in Adj in phase 2L ($p < 0.0001$), but did not differ by phase in Non. IC nuclear position differed from Adj during phases 1E–2E ($p < 0.001$) and from Non during phases 1E–2L ($p < 0.0001$), but did not differ from Adj in phase 2L. Adj nuclear position did not differ from Non during phase 1, but differed during phase 2E ($p < 0.05$) and phase 2L ($p < 0.0001$). All cell classes except IC and Adj differed during phase 2L ($p < 0.0001$). (D) Ratio of apical to basal width. The width ratio differed in IC between phases 1E and 2L ($p < 0.01$), but did not significantly differ between other phases. The width ratio in Adj did not differ between phases 1E–2E but differed at phase 2L ($p < 0.0001$). The width ratio did not differ in Non. During phases 1E–2E, the width ratio differed between IC and Adj ($p < 0.0001$) and between IC and Non ($p < 0.0001$), but did not differ between Adj and Non. During phase 2L, IC and Adj did not differ, but IC and Adj differed from Non ($p < 0.0001$); Inv did not differ from Non, but Edg differed from Non ($p < 0.001$). (E) Apical and basal widths. Comparison of apical width to basal width: Apical and basal cell widths differed from each other in IC ($p < 0.0001$) at all phases, in Adj at phase 1E ($p < 0.05$) and at phase 2L ($p < 0.0001$), but did not differ in Non at any phase. Comparison of cell classes: During phases 1E–2E, apical width differed between IC and Non ($p < 0.0001$), IC and Adj ($p < 0.0001$), but did not differ between Adj and Non. During phase 2L, apical widths of IC and Adj did not differ, but both differed from Non ($p < 0.0001$). During phase 1, basal cell width did not differ between IC, Adj and Non, but differed between IC, Adj and Non during phase 2 ($p < 0.01$). Comparison over time: Apical width in IC and Non did not differ over time, but decreased in Adj during phase 2 ($p < 0.0001$). Basal width did not increase in IC between phases 1E and 1L, but increased between all other phases ($p < 0.0001$). Basal width did not increase in Adj between phase 1E and 1L, but increased between 1L and 2E ($p < 0.05$) and between phases 2E and 2L ($p < 0.0001$). Basal width of Non did not differ over time.
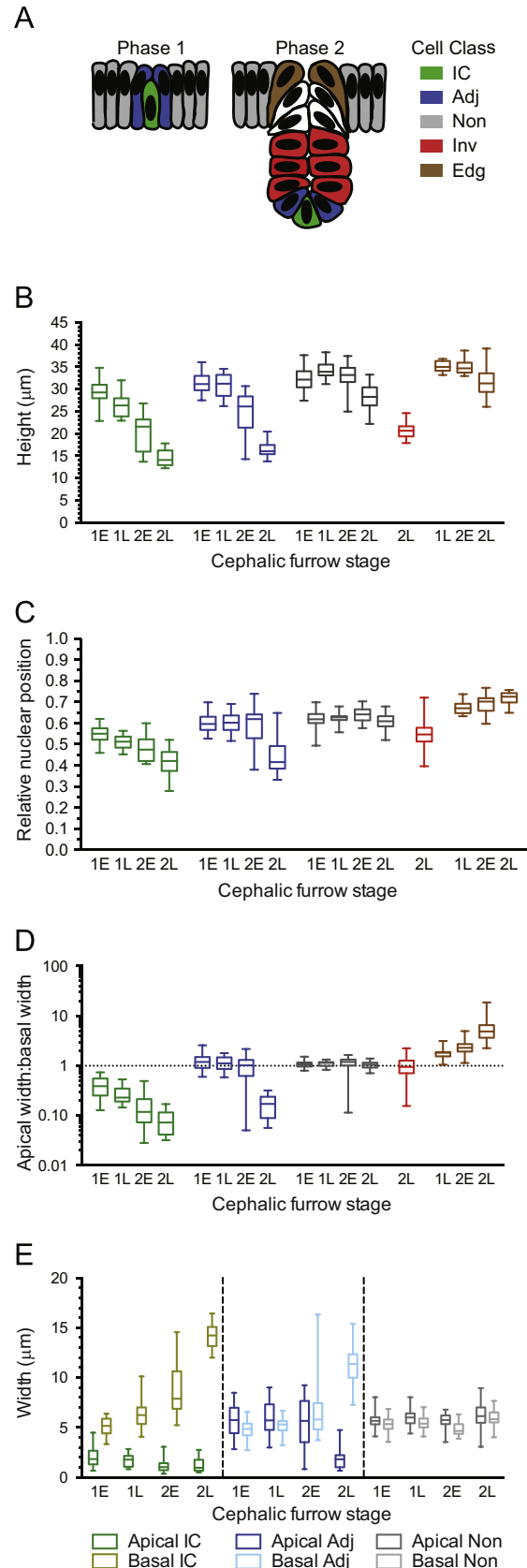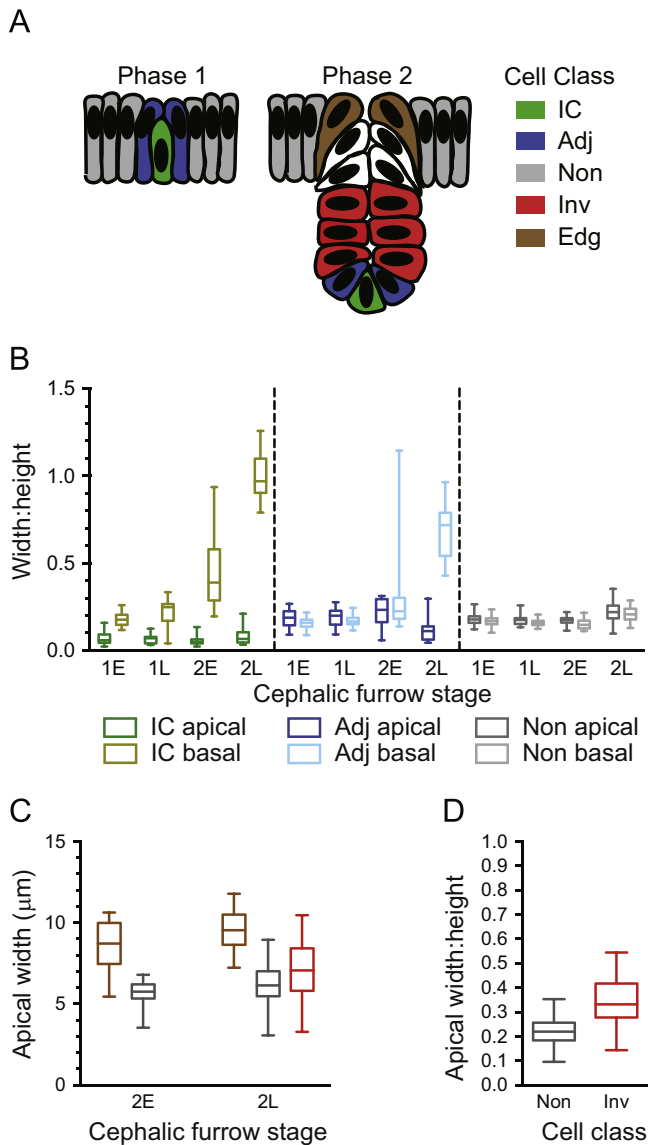
Fig. 4. Cell width changes during early cephalic furrow formation. (A) Diagram of early CF formation showing morphological classes of cells during phase 1 and phase 2 (from Fig. 3A). (B) Comparison of width to height (aspect ratio). Comparison of apical width to basal width: Apical width:height and basal width:height aspect ratios differed from each other in IC at all phases ($p < 0.0001$), in Adj at phase 2E ($p < 0.05$) and phase 2L ($p < 0.0001$), but did not differ in Non. Comparison of cell classes: Throughout phases 1E–2E, the apical width:height aspect ratio differed between IC and Non ($p < 0.001$), and between IC and Adj ($p < 0.0001$). During phase 2L, IC and Adj did not differ, but both differed from Non ($p < 0.0001$). The basal width:height aspect ratio did not differ between IC, Adj and Non during phase 1, but differed between IC, Adj and Non during phase 2 ($p < 0.0001$). Comparison over time: the apical width:height ratio did not differ in IC during phases 1E–2L; Adj differed only in phase 2L ($p < 0.05$). Basal width:height ratios in both IC and Adj did not differ between phases 1E and 1L, but differed at all other time points ($p < 0.0001$). Apical and basal width:height ratios did not differ in Non over time. (C) Comparison of apical widths of invaginated cells, non-invaginated cells and cells at the furrow edge. Apical width of Edg did not change, and was wider than Non ($p < 0.0001$). Apical width of Inv did not differ from Non during phase 2L. (D) Comparison of width to height (aspect ratio) of invaginated and non-invaginated cells at late phase 2. The aspect ratio of Inv differed from that of Non ($p < 0.0001$, two-tailed T-test).

initiator cells was 0.96, consistent with the shape of a squat wedge with approximately equal basal width and height (Fig. 4B). Thus, apical constriction occurred before invagination, whereas basal expansion occurred during invagination. These findings suggest that initiator cell apical constriction and basal expansion are not directly coupled and are likely mechanically independent.

Adjacent cells

The adjacent cells also underwent extensive cell shape changes and became short and wedge-shaped. Despite the similarity to initiator cells in shape during late phase 2, the timing of these cell shape changes was quite different. In contrast to initiator cells, adjacent cells showed little or no shortening in phase 1, but shortened dramatically during phase 2, and by late phase 2 were almost as short as initiator cells (Fig. 3B). Likewise, the nuclei of adjacent cells shifted basally, but later than in initiator cells. The median relative nuclear positions of adjacent cells were similar to those of non-invaginated cells in phase 1, but in late phase 2, the median relative nuclear positions were similar to those of initiator cells (Fig. 3C).

Adjacent cells adopted a wedge shape later than the initiator cells. The median ratio of apical width to basal width was approximately 1.0 until midway through phase 2 (Fig. 3D). However, the median apical to basal width ratio of adjacent cells during late phase 2 was similar to that of initiator cells (Fig. 3D). Like initiator cell wedging, adjacent cell wedging occurred by both apical constriction and basal expansion. During phases 1 and early phase 2, both apical and basal width medians were around 5–6 μm, like non-invaginated cells (Fig. 3E). In late phase 2, the median width of an adjacent cell apex was 1.8 μm and the median base width was 11.3 μm (Fig. 3E). During late phase 2, adjacent cells had a median apical aspect ratio of 0.11 and a median basal aspect ratio of 0.72, indicating that the adjacent cells had become wedge-shaped; however, the wedge shape was not as pronounced as that of initiator cells (Fig. 4B). Strikingly, adjacent cells wedged very rapidly (~ 5 min) compared to initiator cells (~ 15 min) (Fig. 1L, Fig. 3E, Fig. 4B).

Cells that have invaginated into the cephalic furrow

Invaginated cells were columnar, like cells that had not invaginated. Even though non-invaginated cells were shorter during late phase 2 than earlier, invaginated cells were typically 7.5 μm shorter than non-invaginated cells (Fig. 3B). Like non-invaginated cells, invaginated cells were shorter on the anterior side of the CF than on the posterior (data not shown). Nuclei tended to be located in the center of the cell, but position was variable (Fig. 3C). The apices and bases of invaginated cells were generally the same width (Fig. 3D). The apical aspect ratio of invaginated cells was about 1.5-fold greater than that of non-invaginated cells (Fig. 4D).

Cells that are at the edge of the cephalic furrow

Cells at the edge of the CF cleft adopted a distinctive transient morphology: distended with their apices bent toward the CF cleft. The edge cells were slightly elongated (Fig. 3B). Nuclei were positioned more apically than in non-invaginated cells (Fig. 3C). The apices of edge cells were typically 3 μm wider than those of non-invaginated cells (Fig. 4C). The bases of the edge cells were narrower and appeared compressed such that the median apical width of edge cells was about 5-fold greater than the basal width of edge cells at phase 2L (Fig. 3D). This apical expansion and basal narrowing is consistent with a passive deformation of edge cells during CF invagination in response to extrinsic forces. Redistribution of cytoplasm apically might have shifted nuclei apically.

Adherens junction reorganization during early CF formation

We investigated whether adherens junctions were remodeled in CF formation by examining localization of Armadillo (Arm, β-catenin). In non-invaginated cells during late cellularization and early phase 1, Arm was distributed throughout the lateral
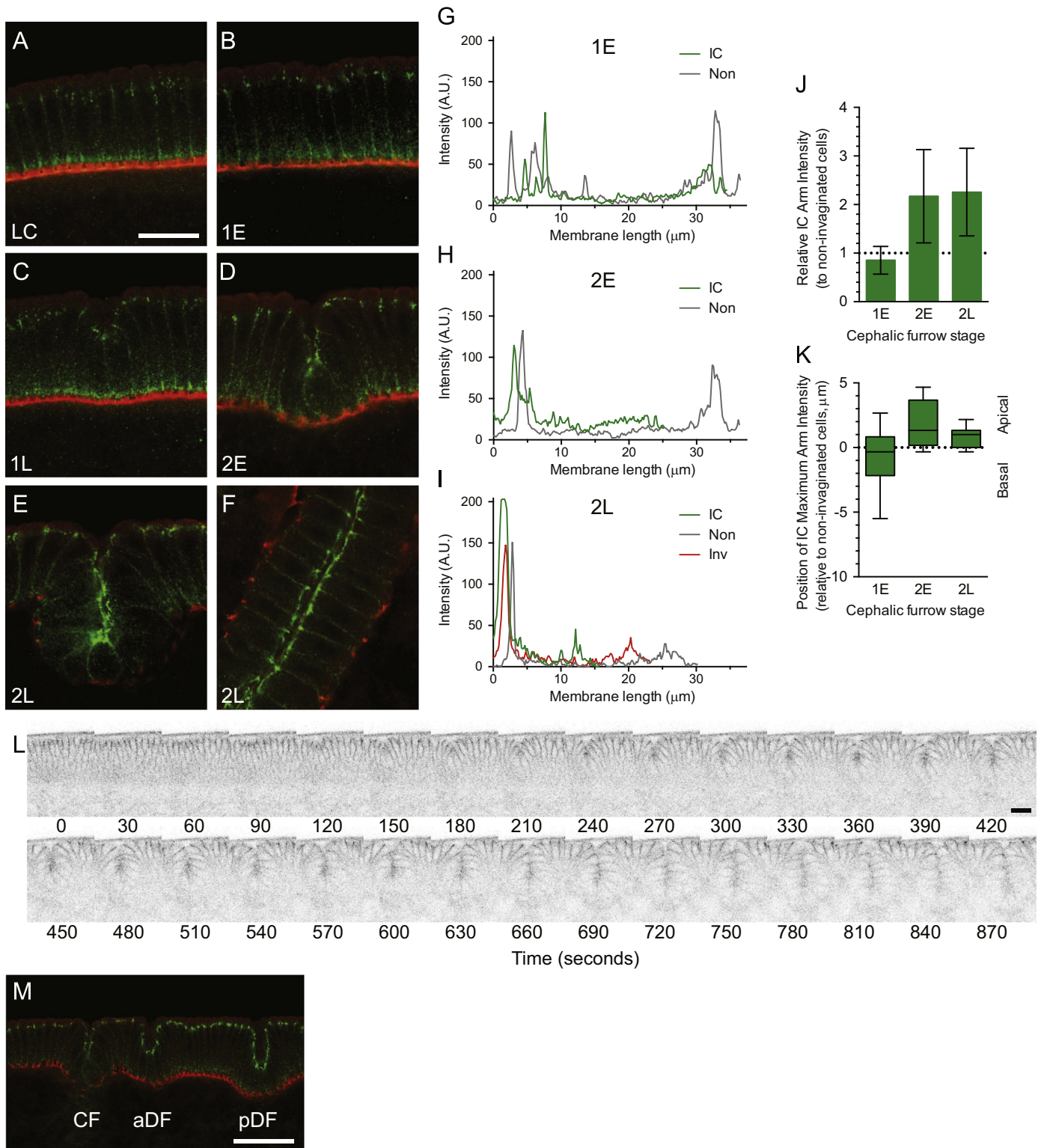
Fig. 5. Adherens junction reorganization during cephalic furrow formation. (A–E) Confocal images showing Arm (green) and Zip (red) to mark cell apices in late cellularization (A), early phase 1 (B), late phase 1 (C), early phase 2 (D) and late phase 2 (E). Scale bar: 20 μm. (F) Sagittal image of CF cleft showing Inv during late phase 2. (G–I) Arm distribution along the cell membrane between the apical contact point and the basal contact point between IC and Adj (green), two Non (gray) and two Inv (red) of representative cells at early phase 1 (G), early phase 2 (H) and late phase 2 (I). Intensity is expressed in arbitrary units (A.U.). (J) Graph showing levels of Arm in initiator cells relative to non-invaginated cells in the apical-most 10 μm in early phase 1 and early phase 2, and in the apical-most 5 μm in late phase 2. Arm levels in IC increased between early phase 1 and phase 2 ($p < 0.01$). Relative intensity was unchanged between early and late phase 2. Error bars: SD. (K) Graph showing relative position of peak intensity of Arm in the apical-most 10 μm in early phase 1 and early phase 2 and in the apical-most 5 μm in late phase 2. Arm was more apical in IC than in Non during early phase 2 ($p < 0.05$), but was not significantly different in early phase 1 or late phase 2. Error bars: SD. (L) Inverted time-lapse montage showing E-cad-GFP during early CF formation (from Supplemental Movie 3). Scale bar: 20 μm. (M) Sagittal image showing cell apices and bases (Zip, red) and Arm (green) of dorsal side of gastrulating embryo. Cephalic furrow (CF), anterior dorsal fold (aDF), posterior dorsal fold (pDF). Scale bar: 40 μm. Anterior: left.

membrane but was concentrated in two regions: the bases of the cells just apical to the furrow canals and the subapical region (Fig. 5A,B and F). Arm localization was distributed over a wide subapical region in all cells in phase 1 (Fig. 5B,C and F). The spot adherens junctions had not coalesced in any cells in phase 1 (Fig. 5B,C).

During phase 2, non-invaginated cells posterior to the CF had a more apical distribution of Arm than non-invaginated cells anterior to the CF (Fig. 5D and E). The amount of Arm found in initiator cell junctions during early phase 2 was twice the amount found in non-invaginated cells (Fig. 5D,H and J). During early phase 2, Arm was more apically localized in initiator cells and adjacent cells that had invaginated into the furrow than in non-invaginated cells (Fig. 5D,H and K). Spot junctions had coalesced by late phase 2 (Fig. 5E,F and I). However, the relative amount of Arm in initiator cells remained twice that of non-invaginated cells (Fig. 5J). During late phase 2, Arm had become more apical in all cells, and did not differ in relative cellular position in initiator cells and in posterior non-invaginated cells (Fig. 5E,F,I and K). After phase 2, Arm became even more apical and condensed further into zona adherens. E-cadherin
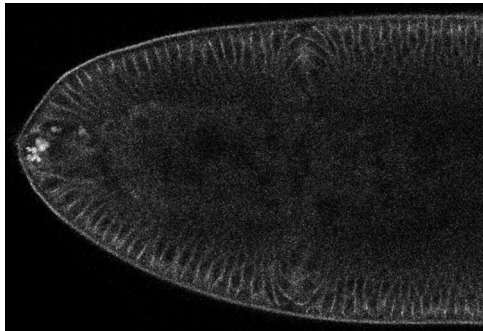
Movie 3. Confocal time-lapse images of D-Ecad-GFP during early CF formation. A video clip is available online. Supplementary material related to this article can be found online at http://dx.doi.org/10.1016/j.ydbio.2015.03.022.

dynamics in live embryos were consistent with Arm staining in fixed embryos (Fig. 5L, Supplemental Movie 3.)

Although superficially similar to the CF, the dorsal folds differed morphologically: the initiating cells of the dorsal fold were tall and less strongly wedge-shaped than the initiator cells of the CF (Fig. 5M) (Wang et al., 2012). Adherens junctions were differentially remodeled: adherens junctions became more apical in initiator cells as CF formation progressed but became more basal in initiating cells as dorsal fold formation progressed (Fig. 5M). (Wang et al., 2012).

Apicobasal polarity complex reorganization during early CF formation

Apicobasal polarity complexes play an important role in the morphogenesis of epithelial tissues, and the *Drosophila* homolog of the Par-3 apical determinant, Bazooka (Baz), is involved in the assembly and positioning of adherens junctions (Bertet et al., 2004; Harris and Peifer, 2004, 2005; Laprise and Tepass, 2011; McGill et al., 2009; Wang et al., 2012; Zallen and Wieschaus, 2004). To determine whether apicobasal polarity complexes were relocalized during CF formation, we investigated Baz localization. At the end of cellularization, Baz was localized to a broad domain in the apical regions of the nascent cells, with more intensely staining puncta in the basal-most part (Fig. 6A) (Harris and Peifer, 2005). During phase 1, Baz remained localized in the same pattern in all cell types; however, it was deeper from the surface in the shorter initiator cells (Fig. 6B and C). Baz distribution was similar at the beginning of phase 2, except that the apical region of lighter Baz staining was more condensed in cells in the CF (Fig. 6D). However, in slightly older phase 2 embryos, the brightly staining Baz puncta were positioned more apically in the initiator and adjacent cells than in non-invaginated cells (Fig. 6E). Baz localization in cells at the edge of the CF cleft was similar to non-invaginated cells, whereas the intensely staining Baz band in invaginated cells was more apically positioned, similar to initiator cells and adjacent cells (Fig. 6E). By late phase 2, Baz had become
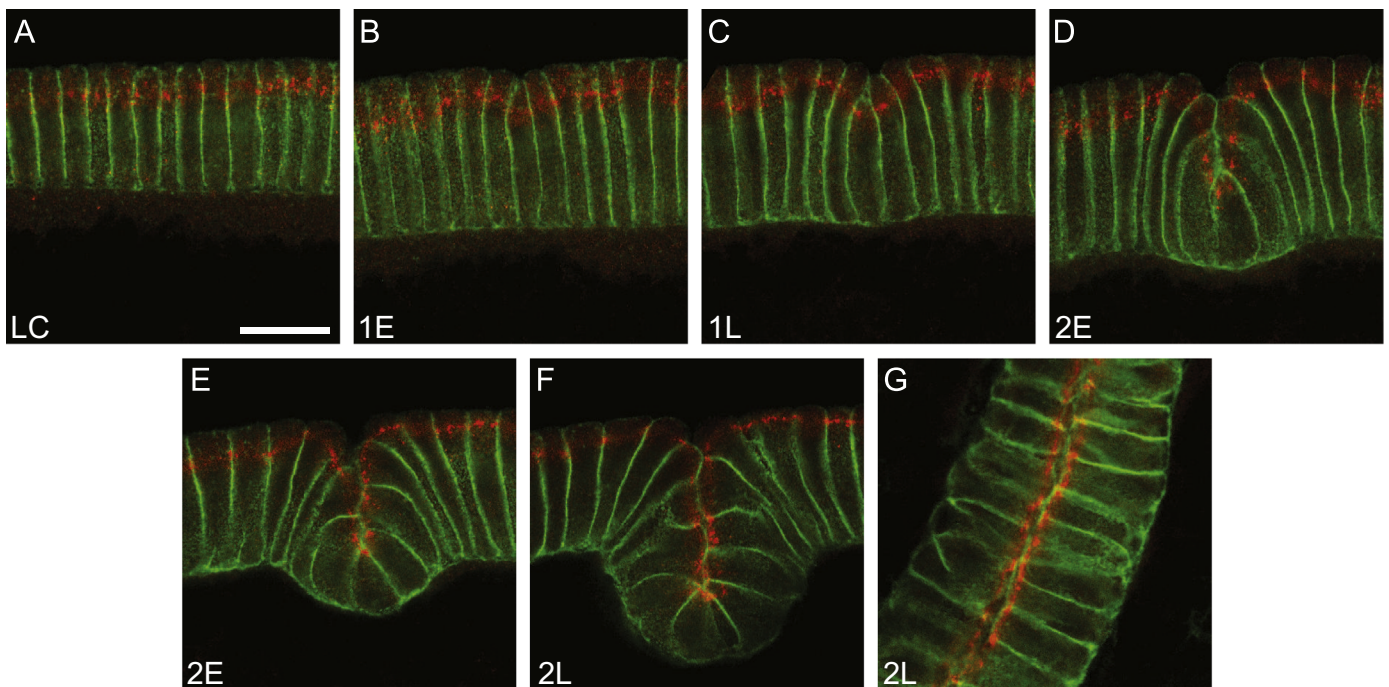

Fig. 6. Apicobasal polarity complex reorganization in the cephalic furrow. (A–F) Confocal images showing Baz (red) and cell membrane (Nrt, green) in late cellularization (A), early phase 1 (B), late phase 1 (C), early phase 2 (D,E) and late phase 2 (F). (G) Sagittal image of CF cleft showing invaginated cells during late phase 2. Scale bar: 20 μm. Anterior: left.

more condensed and more apical in non-invaginated cells, especially the posterior non-invaginated cells (Fig. 6F). The region of intense Baz staining was even more apical in initiator cells and adjacent cells and was very close to the apices (Fig. 6F). Invaginated cells also showed a more apical localization of the brightest region of Baz staining (Fig. 6F and G). Baz distribution in cells at the edge of the cleft was similar to that of non-invaginated cells (Fig. 6F). Thus the transition towards a more apical Baz position in the invaginated cells seems to occur when cells enter the furrow.

Apical myosin II reorganization during early CF formation

Non-muscle myosin II heavy chain (Zip) and myosin regulatory light chain (Sqh) are expressed throughout the embryo during gastrulation (Dawes-Hoang et al., 2005; Young et al., 1991). Since myosin II is a likely driver of cell shape change (Sawyer et al., 2010), we investigated the distribution of myosin II in the developing CF. Zip was present at high levels at the bases of all cells during late cellularization and most of early CF formation; however, Zip levels at the bases declined strikingly in late phase 2 (Fig. 7A–E) (Dawes-Hoang et al., 2005). Although low compared to levels at the cell bases, apical Zip levels were higher than lateral Zip levels in all cells throughout early CF formation (Fig. 7B–F). Neither relative apical levels nor relative apical position of Zip changed in initiator cells, adjacent cells or invaginated cells during CF formation (Fig. 7B–E). However, posterior non-invaginated cells showed slightly increased apical Zip during phase 2 (Fig. 7E), consistent with epithelial reorganization in the trunk (Bertet et al., 2004; Zallen and Wieschaus, 2004).

Sqh-GFP localization in live embryos differed somewhat from Zip localization in fixed embryos. Myosin aggregates were observed at some time points during time-lapse imaging (Fig. 7G, Supplemental Movie 4). To further investigate, we imaged Sqh-GFP en-face over several time points. As CF formation progressed during phase 1, Sqh-GFP was observed in punctate aggregates in the medioapical and subapical membrane regions of the initiator cells and the adjacent cells (Fig. 7H and I). Apical myosin levels increased in the initiator cells as CF formation progressed; however, medioapical myosin did not increase (Fig. 7H,J and K). The subapical region membrane accumulated Myosin II in punctate aggregates that increased in number and intensity as CF formation progressed. Many of the puncta were found at cell vertices (Fig. 7H,I,L and M). Myosin accumulation was polarized: more myosin accumulated in the initiator cell membranes along the CF cleft on the anterior and posterior sides than on the dorsal and ventral sides (Fig. 7 H,I and L). Strikingly, the posterior adjacent cells showed polarized myosin accumulation not only along the anterior sides juxtaposed with the initiator cells, but also along the posterior sides juxtaposed with non-invaginated cells (Fig. 7H,I

and M). These results suggest that subapical accumulation of myosin in both the initiator cells and the adjacent cells may be a response to tension caused by the shortening and apical constriction of the initiator cells.

To determine whether myosin II is active, we stained embryos with antibodies that recognized specific phosphorylated forms of Sqh (Zhang and Ward, 2011). First, we analyzed the localization of Sqh monophosphorylated on Ser21 (Sqh1P). During gastrulation, Sqh1P expression largely corresponded to the expression patterns of Sqh and Zip (Zhang and Ward, 2011). Sqh1P remained enriched basally throughout phase 1, but dropped during phase 2 and basal levels were indistinguishable from cytoplasmic levels during late phase 2 (Fig. 7N–Q). Apical Sqh1P levels in the initiator cells and adjacent cells did not differ from non-invaginated cells throughout early CF morphogenesis (Fig. 7 N–Q). Although phosphorylation at Ser21 is the predominant mechanism of myosin II activation, diphosphorylation on both Ser21 and Thr20 (Sqh2P) might be required to activate Sqh during apical constriction in initiator cells. Diphosphorylation is less common than Ser21 monophosphorylation and is associated with increased activity of myosin (Ikebe and Hartshorne, 1985; Ikebe et al., 1986, 1988). We did not observe apical Sqh2P in any cell type during CF formation (Fig. 7R-U). These results show that there is little apical myosin II activation during CF formation. However, phosphorylated Sqh staining is weak in early embryos (Zhang and Ward, 2011).

The apical actin cytoskeleton is reorganized during early CF formation

To determine whether actin remodeling has a role in CF formation, we stained gastrulating embryos with fluorescently labeled phalloidin to visualize F-actin. At the beginning of gastrulation, the strongest phalloidin staining was observed in the furrow canals at the bases of the blastoderm cells (Fig. 8A and B). Elsewhere, F-actin was primarily found in the cell cortex during CF formation (Fig. 8A–E). In non-invaginated cells, F-actin was less abundant (about 70%) in the apical regions that do not contact other cells than in the basolateral cortex, and remained unaltered throughout early CF formation (Fig. 8A–F). Initiator cell apical F-actin levels increased throughout early CF formation, and by late phase 2, were more than twice initiator cell basolateral F-actin levels, and about 6.9-fold more than non-invaginated cell apical F-actin levels (Fig. 8A–G). F-actin levels also increased in the apices of adjacent cells throughout phase 2 (Fig. 8A–G). In phase 2, F-actin levels in adjacent cell apices were similar to those in initiator cell apices (Fig. 8D–G). During phase 2, apical F-actin levels in cells at the edge of the furrow cleft were similar to those in non-invaginated cells, whereas apical F-actin levels in invaginated cells were similar to apical F-actin levels in initiator cells and adjacent cells (Fig. 8E–G). Basolateral levels of F-actin in initiator

Fig. 7. Myosin II during cephalic furrow formation. (A–E) Confocal images showing non-muscle myosin II heavy chain (Zip) (from Fig. 5A–E), in late cellularization (LC), early phase 1 (B), late phase 1 (C), early phase 2 (D) and late phase 2 (E). (F) Sagittal image of CF cleft in late phase 2. (G) Inverted time-lapse montage showing myosin regulatory light chain-GFP (Sqh-GFP) localization during phase 1 (from Supplemental Movie 4). (H) Inverted *en-face* maximum intensity z-stack projections of images of medioapical and subapical Sqh-GFP at different time points before and after the start of initiator cell shortening at 0 min. (I) *en-face* z-stack projections of the subapical region showing cell membrane (Spider-GFP, green) and myosin (Sqh-mCherry, red) after initiator cell shortening has started. (J) Graph showing total levels of apical Sqh-GFP relative to non-invaginated cells in initiator cells (green) and adjacent cells (blue) before and after the start of initiator cell shortening at 0 min. Initiator cell Sqh-GFP levels differ between −2 min and 2 and 4 min ($p < 0.01$), and 0 and 4 min ($p < 0.05$). Adjacent cell Sqh-GFP levels differ between −2 min and 4 min ($p < 0.05$). Error bars: SD. (K) Graph showing medioapical levels of Sqh-GFP relative to non-invaginated cells in initiator cells (green) and adjacent cells (blue) before and after the start of initiator cell shortening at 0 min. Levels do not differ over time. Error bars: SD. (L) Graph showing subapical levels of Sqh-GFP relative to non-invaginated cells in initiator cells, before and after the start of initiator cell shortening at 0 min, by angle relative to the anteroposterior axis at 0°. Sqh-GFP levels at 0 min are greater in cell faces at 60–90° than at 0–30° ($p < 0.01$), Sqh-GFP levels at 2 min and 4 min are greater at 60–90° than at either 0–30° ($p < 0.05$) or 30–60° ($p < 0.01$). Sqh-GFP levels increased in initiator cell faces at 30–60° from −2 min to 0 min and 2 min ($p < 0.05$), and cell faces at 60–90° from −2 min to 0 min ($p < 0.05$) and to 2 min and 4 min ($p < 0.0001$). 30: 0–30°, 60: 30–60°, 90: 60–90°. Error bars: SD. (M) Graph showing subapical levels of Sqh-GFP relative to non-invaginated cells in adjacent cells, before and after the start of initiator cell shortening at 0 min, by angle relative to the anterior-posterior axis at 0°. Sqh-GFP levels at 2 min and 4 min are less in cell faces at 0–30° than at 30–60° ($p < 0.05$) and 60–90° ($p < 0.001$). Sqh-GFP levels increased in adjacent cell faces at 30–60° from −2 min to 2 min ($p < 0.05$) and 4 min ($p < 0.01$), and cell faces at 60–90° from −2 min to 2 min ($p < 0.01$) and 4 min ($p < 0.0001$) and from 0 min to 4 min ($p < 0.01$). 30: 0–30°, 60: 30–60°, 90: 60–90°. Error bars: SD. (N–Q) Confocal images of early CF formation showing monophosphorylated myosin regulatory light chain at Ser21 (Sqh1P) in early phase 1 (N), late phase 1 (O), early phase 2 (P) and late phase 2 (Q). (R–U) Confocal images of early CF formation showing diphosphorylated myosin regulatory light chain at Thr20 and Ser21 (Sqh2P) in early phase 1 (R), late phase 1 (S), early phase 2 (T) and late phase 2 (U). Scale bars: 20 μm. Anterior: left.
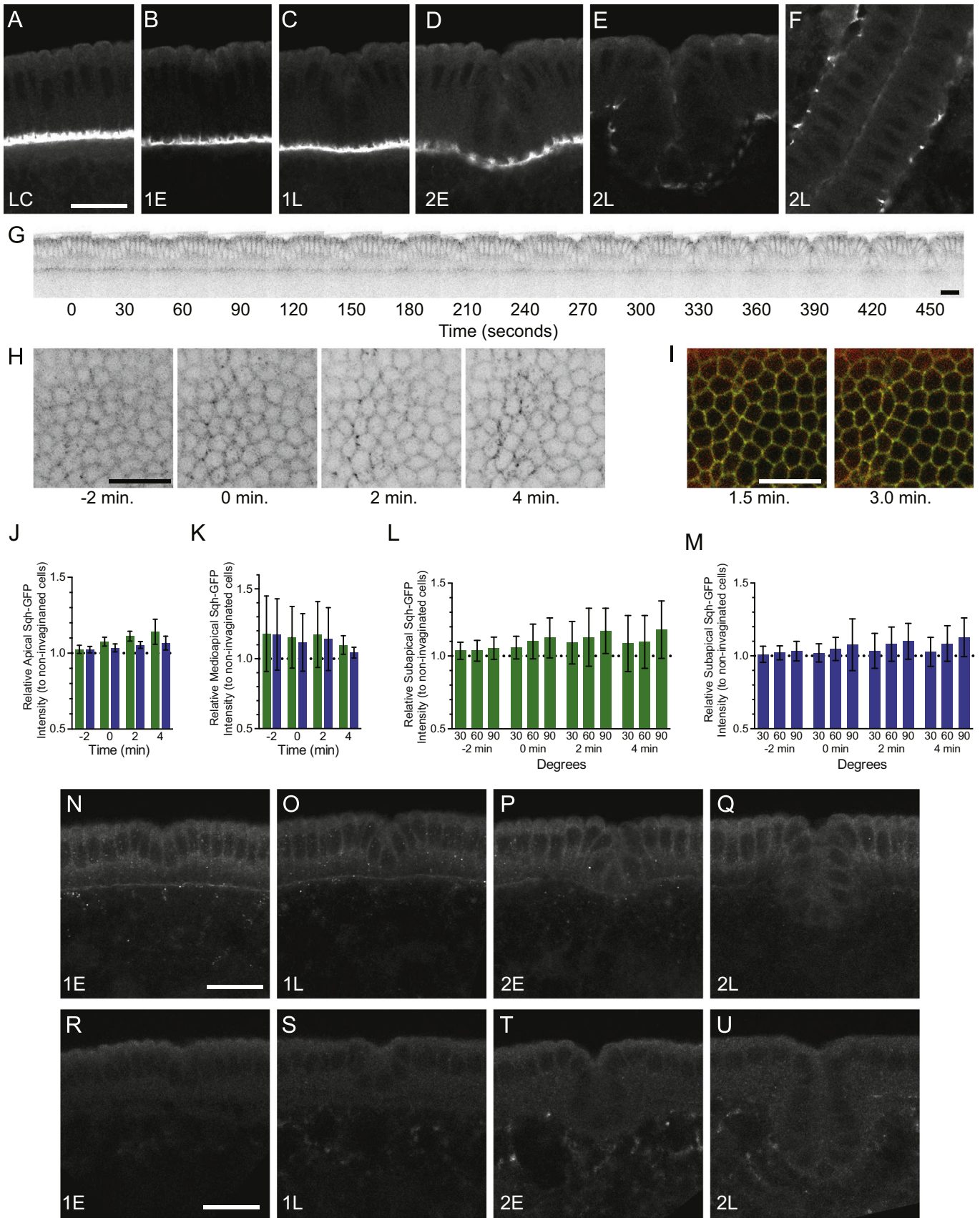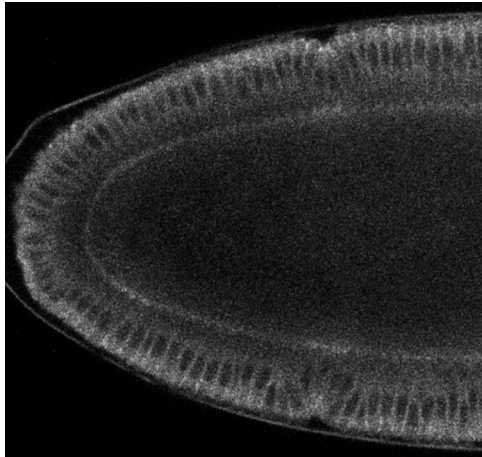
Movie 4. Confocal time-lapse images of Sqh-GFP during early CF formation. A video clip is available online.Supplementary material related to this article can be found online at http://dx.doi.org/10.1016/j.ydbio.2015.03.022.

cells and adjacent cells increased between phase 1 and late phase 2 (Fig. 8E and H). F-actin dynamics were visualized using the F-actin binding domain of moesin tagged with GFP (sGMCA) (Kiehart et al., 2000). sGMCA redistribution during CF formation was consistent with phalloidin redistribution observed in fixed embryos (Fig. 8I, Supplemental Movie 5). These results show that actin is remodeled in the apices of the initiator cells during cell shape change and invagination of the CF in phases 1 and 2, and in the apices of adjacent cells and invaginated cells during CF invagination in phase 2.

Discussion

Apical constriction and actomysosin contraction in the cephalic furrow

Apical constriction is associated with, and thought to drive, many epithelial invaginations during development, even in
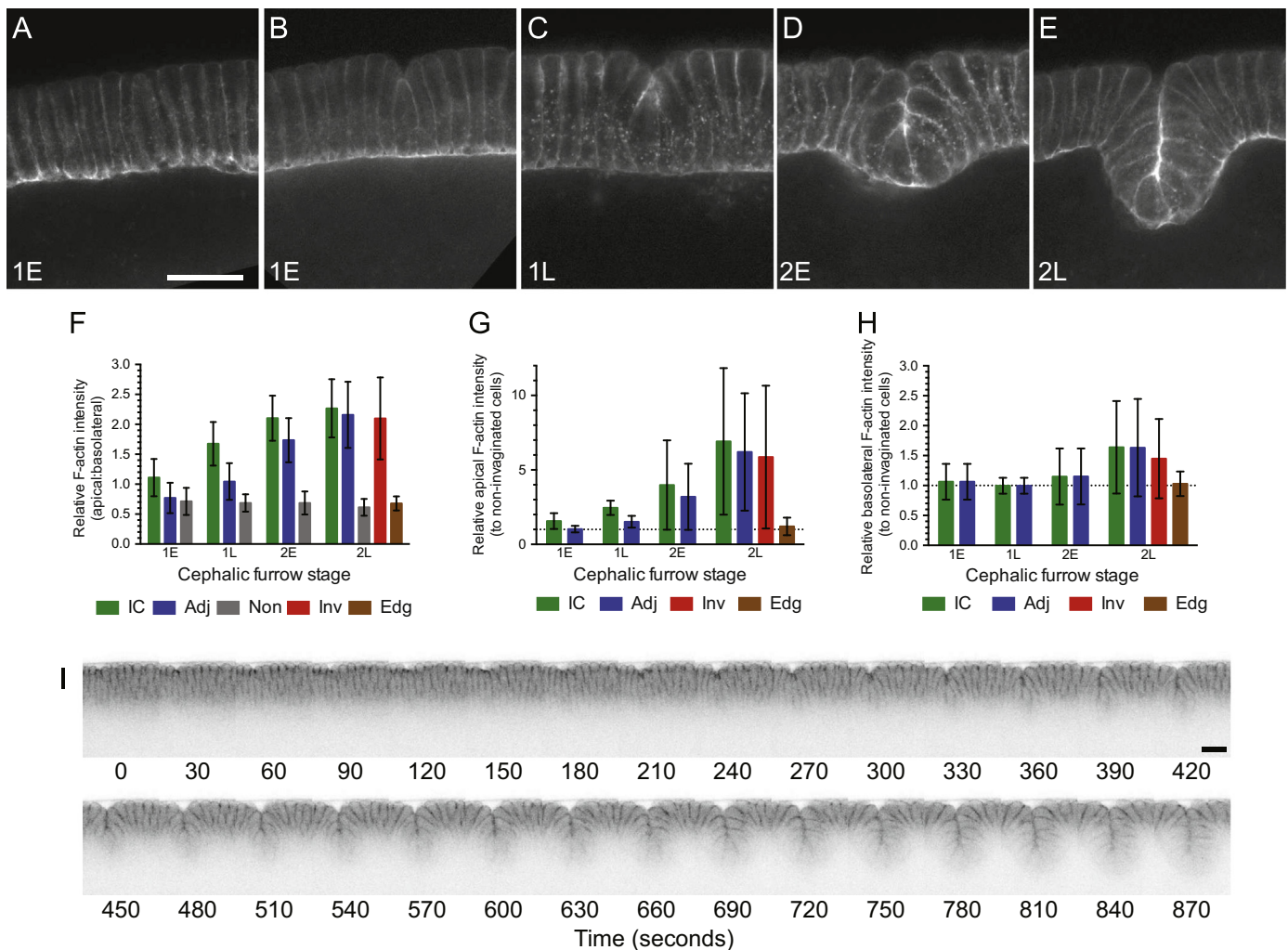

Fig. 8. F-actin reorganization in the cephalic furrow. (A–D) Confocal images of early CF formation showing F-actin (phalloidin, green) and nuclei (Hoechst, blue) in early phase 1 (A,B), late phase 1 (C), early phase 2 (D) and late phase 2 (E). (F) Graph showing relative apical to basolateral F-actin levels. Apical F-actin levels increased relative to basolateral F-actin in IC from early phase 1 to phase 2 ($p < 0.0001$), and in Adj from early phase 1 to phase 2 ($p < 0.0001$). Relative apical to basolateral F-actin levels were unchanged in Non throughout CF formation. Relative apical to basal F-actin levels differed between IC and Non during late phase 1 to late phase 2 ($p < 0.0001$), and between Adj and Non during early phase 2 and late phase 2 ($p < 0.0001$), but did not differ between IC and Adj during phase 2. Relative apical to basolateral F-actin levels in Inv differed from those of Non and Edg ($p < 0.0001$), but not IC or Adj at late phase 2. Error bars: SD. (G) Graph showing apical F-actin levels in different cell types relative to apical F-actin levels in Non. Apical F-actin levels in both IC and Adj relative to Non differed between phase 1 and late phase 2 ($p < 0.01$). Relative apical F-actin levels did not differ between IC and Adj. At late phase 2, Inv did not differ from IC or Adj, and IC, Adj and Inv all differed from Edg ($p < 0.05$). Error bars: SD. (H) Graph showing basolateral F-actin levels relative to Non. Basolateral F-actin levels differed between phase 1 and late phase 2 for both IC and Adj ($p < 0.05$). Error bars: SD. (I) Inverted time-lapse montage of sGMCA during early CF formation (from Supplemental Movie 5). Scale bars: 20 μm. Anterior: left.
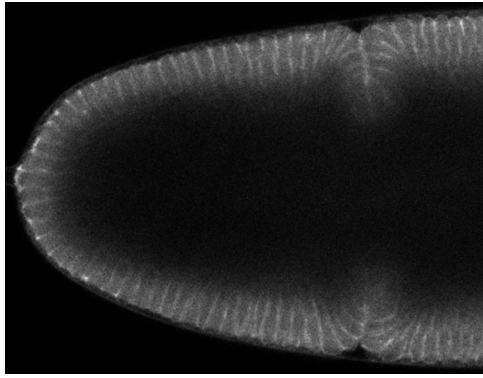
Movie 5. Confocal time-lapse images of sGMCA during early CF formation. A video clip is available online.Supplementary material related to this article can be found online at http://dx.doi.org/10.1016/j.ydbio.2015.03.022.

cnidarians and *Volvox* (Davidson et al., 1995; Ettensohn, 1985; Fristrom, 1988; Hohn and Hallmann, 2011; Keller et al., 2003; Larsen et al., 2003; Lecuit and Lenne, 2007; Magie et al., 2007; Martin and Goldstein, 2014; Martin et al., 2009; Odell et al., 1981; Sawyer et al., 2010; Sherrard et al., 2010; Viamontes and Kirk, 1977). Actomyosin contraction appears to be the predominant mechanism that drives apical constriction (Martin and Goldstein, 2014; Plageman et al., 2010; Sawyer et al., 2010; Sherrard et al., 2010). Increased myosin II levels and increased phosphorylation of myosin regulatory light chain in the apices of cells undergoing apical constriction during epithelial invagination have been observed in gastrulation, in vertebrate neural tube folding, and in other invaginations (Plageman et al., 2010; Sawyer et al., 2010; Sherrard et al., 2010; Simoes et al., 2006; Zhang and Ward, 2011). We observed a modest increase in subapical junctional myosin II levels in apically constricted initiator cells, but observed no change in medioapical myosin II levels. The absence of a change in medioapical myosin II suggested that medioapical actomyosin contraction does not drive apical constriction in initiator cells.

Myosin contraction occurs along the length of the actomyosin filament. This mechanism is observed in cell intercalation during *Drosophila* germ band extension, and in the polarized apical constriction of neuroepithelial cells that bend the neural tube, where phosphorylated myosin is enriched along the axis of apical constriction (Bertet et al., 2004; Blankenship et al., 2006; Nishimura et al., 2012; Nishimura and Takeichi, 2008). Strikingly, we observed Sqh-GFP accumulation in punctate aggregates in the initiator cell faces oriented along the dorsoventral axis, perpendicular to the direction of polarized apical constriction of the initiator cells. Thus, myosin II is enriched in the opposite direction of cell constriction. This suggests that myosin II is not driving apical constriction in initiator cells, but instead accumulates in response to another force driving polarized apical constriction. We propose that the enrichment of myosin II in punctate aggregates, presumably at spot adherens junctions of the initiator cells, acts to resist tension on the initiator cell to maintain cell integrity. Similarly, polarized punctate myosin II accumulations are observed on cell membranes along the dorsoventral axis on both sides of the adjacent cells, which are subjected to apical stretching caused by the pulling force of initiator cells shortening, and thus likely act to resist the tension generated by initiator cell shortening and apical constriction. Therefore, our results suggest that actomyosin contraction is not responsible for apical constriction of initiator cells.

Theoretical and modeling studies have suggested other possible mechanisms for apical constriction (Davidson et al., 1995; Ettensohn, 1985; Keller et al., 2003). Apical constriction during CF formation could be an active cell-intrinsic process or a passive response to cell-extrinsic forces. An alternative, active cell-intrinsic mechanism of apical constriction is seen in the formation of the dorsal transverse folds during *Drosophila* gastrulation. Here, apical constriction occurs without an increase in apical Sqh levels, but requires repositioning adherens junctions more basally through apicobasal polarity remodeling (Wang et al., 2012, 2013). In contrast, we observed that adherens junctions were repositioned more apically in initiator cells during CF formation. Apical constriction as a passive response to a cell-extrinsic force is seen in the invagination of tracheal pits. The central cells of the tracheal placode undergo cell rounding during mitosis; contraction of circumferential actomyosin cables in surrounding cells creates an external pushing force that causes the central cells to undergo apical constriction (Kondo and Hayashi, 2013). Thus, cytoskeletal remodeling could reduce a cell's resistance to external forces that drive passive apical constriction.

Apical constriction might not have a mechanistic role in CF formation, but instead might be a permissive factor in CF invagination. Regardless of the means of their formation, the geometry of wedge-shaped cells in an epithelial sheet facilitates its bending and thus invagination (Ettensohn, 1985; Llimargas and Casanova, 2010). Apical constriction has been proposed to function in the spatiotemporal control of invagination (Llimargas and Casanova, 2010). Thus, apical constriction of the row of initiator cells might establish a precise position and time for the embryonic blastoderm to fold inwards. This is consistent with the separation in time observed between apical constriction of initiator cells and CF invagination. It is also consistent with the observation that *eve* mutants, which abolish initiator cell fate specification and apical constriction, undergo a late and disorganized CF invagination (Vincent et al., 1997).

Adherens junctions

Adherens junctions are a defining feature of epithelia and are essential for maintaining the integrity of the cell sheet, for transmitting and resisting force, and for morphogenesis (Baum and Georgiou, 2011; Harris and Tepass, 2010; Lecuit and Lenne, 2007; Lecuit et al., 2011). At the start of gastrulation, adherens junctions are not yet fully mature and consist only of spot adherens junctions; as gastrulation progresses, spot adherens junctions start to become zona adherens (Tepass and Hartenstein, 1994). Adherens junctions have been shown to be involved in maintaining epithelial integrity during gastrulation (Harris and Peifer, 2004). Adherens junctions mature early in invaginating cells in the posterior midgut and ventral furrow, and are essential for effective actomyosin contraction-driven apical constriction in the cells of the ventral furrow (Dawes-Hoang et al., 2005; Martin et al., 2010; Sawyer et al., 2009; Spahn et al., 2012; Tepass and Hartenstein, 1994).

Arm became more apically located in initiator cells and invaginated cells than in non-invaginated cells during early phase 2. Also, the amount of Arm in adherens junctions had doubled in initiator cells relative to non-invaginated cells during phase 2. These observations suggest that adherens junction remodeling is not very important for apical constriction during phase 1 of CF formation, but that adherens junctions remodeling is important for CF invagination during phase 2. More mature adherens junctions are likely needed to resist the tensile stresses caused by cell shape change and invagination, and maintain epithelial integrity during CF formation. These stresses might stimulate the maturation of adherens junctions (Lecuit et al., 2011). Reduction of E-cadherin levels at adherens junctions by mutation of the glucosyltransferase encoded by *xiantuan* (*xit*) gene led to abnormalities in both ventral furrow and cephalic furrow formation (Zhang et al., 2014), suggesting that E-cadherin is required for proper CF formation.

Potential roles of F-actin reorganization

We observed increased apical F-actin in the CF. This is consistent with the observation that several WASP family proteins are enriched in the CF (Rodriguez-Mesa et al., 2012). Increased apical F-actin in apically constricting initiator cells suggests the possibility that F-actin remodeling, rather than actomyosin contraction, might cause apical constriction during CF formation. Also, asymmetric remodeling of F-actin in initiator cell apices may facilitate constriction along one axis but not the other, producing a wedge instead of a pyramid. Alternatively, enrichment of F-actin in initiator cell apices may be simply the consequence of the same amount of F-actin occupying a smaller area in the constricted apex, and thus has no mechanistic role in apical constriction or initiator cell shape change.

Apical F-actin remodeling might produce a force involved in CF invagination during phase 2. F-actin increased in the apices of cells that invaginated after the initiator cells. These cells become shorter and wider, but do not apically constrict. Expansion of the apical cortical actin cytoskeleton by polymerization of F-actin could drive the change to wider, shorter cells in the furrow and thereby contribute to the invagination of the CF. Similar cell shape changes driven by actin polymerization contribute to tentacle and body column elongation in the cnidarian *Nematostella vectensis* (Fritz et al., 2013). Alternatively, arrangement of F-actin into filopodia or lamellipodia at the apices of invaginating cells could generate protrusive or traction forces to help drive CF invagination (Jacinto et al., 2000; Kress et al., 2007; Lecuit et al., 2011; Mammoto and Ingber, 2010; Millard and Martin, 2008; Pollard and Borisy, 2003).

Cell shape change and potential mechanisms of cephalic furrow morphogenesis

The dynamics of cell wedging differ in different invaginations (Keller et al., 2003; Keller and Shook, 2011). In the first step of *Drosophila* ventral furrow formation and ascidian endoderm invagination, cells constrict their apices and concomitantly elongate apicobasally; in a second step, cells shorten apicobasally and expand basally (Kam et al., 1991; Leptin and Grunewald, 1990; Sherrard et al., 2010; Sweeton et al., 1991). During dorsal lip invagination of *Xenopus* gastrulation, the leading cells undergo concomitant apical constriction, apicobasal elongation and basal expansion (Hardin and Keller, 1988; Keller et al., 2003; Lee and Harland, 2007). These examples are in marked contrast to the dynamics of cell wedging in initiator cells during CF formation. In phase 1, initiator cells undergo concomitant apical constriction and apicobasal shortening. In phase 2, apicobasal shortening continues, accompanied by basal expansion.

Apicobasal shortening starts at the beginning of CF formation in the initiator cells, and we postulate that it is an active cell-intrinsic process that drives initiator cell shape change (Davidson et al., 1995; Keller et al., 2003; Sherrard et al., 2010). Although apical constriction occurs during cephalic furrow formation, it is not as pronounced as apicobasal shortening or basal expansion. Constriction of the initiator cell apices may be a passive deformation caused by initiator cell shortening and adherence to the adjacent cells. Active apicobasal shortening and passive apical constriction followed by active apicobasal shortening with basal expansion should be sufficient to drive initiator cell wedging. Basal expansion of the initiator cells during phase 2 could be either an active cell-intrinsic process or a passive deformation caused by apicobasal shortening. In phase 2, the adjacent cells undergo cell wedging. The rapid apicobasal shortening and apical constriction of adjacent cells are consistent with a passive deformation driven by forces produced by both initiator cell shape change and tissue invagination. We postulate that active apicobasal shortening is specific to initiator cells and is regulated by mechanisms established by the adoption of the initiator cell identity. The key regulatory proteins are likely transcribed zygotically in response to Eve and Btd expression (Vincent et al., 1997).

Force generation coupled with cell volume conservation can cause cell shape change in the embryo (Gelbart et al., 2012). Initiator cell shortening and apical constriction occur without basal expansion during phase 1 before invagination begins. These cell shape changes suggest that cytoplasmic volume is not conserved during phase 1. Yolk stalks maintain open channels between cells and the yolk sac during early gastrulation (Gelbart et al., 2012; Rickoll, 1976). The yolk stalks remain open to the yolk sac in CF cells into early phase 2 (Fig. 1 M–O). We propose that initiator cell shortening leads to cytoplasmic loss and a reduction of volume of the initiator cells during phase 1. Initiator cell shortening continues during phase 2 and basal expansion starts at the beginning of phase 2. We propose that apical shortening drives rapid basal expansion during phase 2 by forcing cytoplasm basally when the yolk stalk channels are closed and cell volume is constant. The initiator cell apex remains constricted when the basal region of the cell expands, forming a shortened wedge shape.

Initiator cell-intrinsic forces are likely sufficient to drive CF invagination partway through phase 2. Widening of invaginated cells driven by F-actin remodeling may drive further invagination of the CF during phase 2 and beyond. The CF continues to invaginate after phase 2 of CF invagination (Campos-Ortega and Hartenstein, 1997). Initiator cell wedging would be insufficient to drive the deepening of the CF in this later period of development, suggesting that other, extrinsic forces drive deeper CF invagination. Multiple forces may drive CF invagination. In addition to forces generated by cell widening, other extrinsic forces might include those generated by the cell intercalation driving germband extension, which could push trunk cells into the CF, and cell division during late CF invagination. Ultrastructural studies of gastrulating embryos show a gap between CF cell bases and the underlying yolk sac membrane, and yolk stalks positioned in the centers of initiator cells and close to the deepest part of CF invagination in other cell types, consistent with the existence of a pulling force originating from the yolk sac (Rickoll, 1976; Rickoll and Counce, 1980). At present, it is unclear which potential forces make a contribution to CF invagination. Overall, our results suggest that CF formation differs from other well-characterized epithelial invaginations and that novel mechanisms are involved. Further investigation should provide new insights into the morphogenesis of epithelial tissues during development.

Materials and methods

Fly strains and genetics

OreR was used as the wild-type strain. For live imaging experiments, the following stocks were used: *Spider-GFP* (Morin et al., 2001), *sqh^{AX3}; sqh-GFP* (myosin regulatory light chain–GFP) (Royou et al., 2002), *sqh-mCherry; Spider-GFP* ((Martin et al., 2009)), *H2A-mRFP* (histone-RFP) (St Pierre et al., 2014), *sGMCA* (actin-binding subunit from moesin) (Kiehart et al., 2000), *shg-GFP* (E-cadherin-GFP, DGRC, Kyoto) (Oda and Tsukita, 2001). Embryos from *Spider-GFP/+; H2A-mRFP/+* mothers were used for dual imaging of cell membrane and nuclei. Embryos from *sqh-mCherry/+; Spider-GFP* mothers were used for dual imaging of cell membrane and myosin.

Immunofluorescence

To visualize myosin heavy chain, Armadillo, E-cadherin, Neurotactin and Bazooka, embryos were heat-methanol fixed (Muller and Wieschaus, 1996). Antibodies used were rabbit anti-Zip (A. Chougule and J.H. Thomas, unpublished, using a clone produced by A. Sokac, 1:500) (Sokac and Wieschaus, 2008), mouse anti-Arm (N27A1, Developmental Studies Hybridoma Bank (DSHB) 1:50), mouse anti-Nrt (BP106, DSHB, 1:10), and rabbit anti-Baz (1:500) (Wodarz et al., 1999). To visualize Ser21 monophosphorylated Sqh, embryos were fixed in 4% paraformaldehyde for 20 min and stained with guinea pig anti-Sqh1P (1:500) (Fehon et al., 1994; Zhang and Ward, 2011). To visualize diphosphorylated Sqh, embryos were fixed in cold 10% trichloroacetic acid and stained with rat anti-Sqh2P (1:2000) (Zhang and Ward, 2011). Alexafluor 488- and Alexafluor 546-coupled goat secondary antibodies (Molecular Probes) were used. F-actin was visualized with Alexafluor 488-conjugated phalloidin (Molecular Probes) in formaldehyde-fixed embryos that were devitellinized by hand with a hypodermic needle (Wieschaus and Nüsslein-Volhard, 1998). For morphological analyses, embryos were manually oriented in Aquapolymount (Polysciences) on a coverslip, and allowed to dry before mounting the coverslip on a slide with Aquapolymount. Imaging was performed with either a Zeiss AxioImager.A1 fluorescence microscope or an Olympus Fluoview 300 laser-scanning confocal microscope.

Scanning electron microscopy

Embryos were dechorionated in 50% bleach and fixed in 4% formaldehyde-PBS/heptane for 20 min, devitellinized by shaking in 1:1 heptane:methanol and rinsed in methanol. Embryos were rehydrated by washing twice in 1% BSA/PBS-0.1% Triton X-100 for at least 40 min and rinsed in PBS/0.1% Tween 20. Rehydrated embryos were fixed in 25% glutaraldehyde in PBS for 30 min and washed in PBS/Tween 20. Embryos were dehydrated in an ethanol series (30 min each at 30%, 50%, 70%, 90%, 95% and 100%) and incubated in hexamethyldisilazane (HDMS) for 10 min. HMDS was removed and embryos were allowed to dry before orientation and mounting. Embryos were sputtercoated with gold and imaged at 10 kV using a Hitachi S-3400N SEM. Embryos were staged by morphology (Campos-Ortega and Hartenstein, 1997; Spahn et al., 2012).

Live imaging

Live embryos were dechorionated in 50% bleach for 2 min, washed and mounted in halocarbon oil 27 (Sigma) on biofoil membrane and visualized through a number 1.5 coverslip supported by two number 1 coverslips on each side as described (Thomas and Wieschaus, 2004). For bright-field time-lapse imaging, images were collected every 20 sec. using a Zeiss AxioImager. A1 microscope. For confocal time-lapse imaging, images were collected every 5 s using an Olympus FV 300 confocal microscope. For *sGMCA* imaging, the pinhole was opened. For *en-face* imaging of *sqh-GFP* and *sqh-mCherry; Spider-GFP*, embryos were glued to coverslips and covered with halocarbon oil 27 (Cavey and Lecuit, 2008; Martin et al., 2009).

Image analysis

Apical depth and invagination depth were measured as the distance from the initiator cell apex to the blastoderm cell apices, and as the distance from the initiator cell base to the bases of the blastoderm, respectively, using Axiovision 4.4 (Zeiss). Images and time-lapse series were analyzed using ImageJ (W. Rasband, NIH,

http://rsb.info.nih.gov/ij/). *en-face* still images were taken from z-stacks of 0.5 μm steps. Measurements of cells other than the initiator cells were conducted on cells posterior to the initiator cells. Cell height was measured as the length of the line segment from the center of the cell apex to the center of the cell base. Usually the line segment was perpendicular to the plane of the cellular blastoderm but deviated in edge cells and adjacent cells that bend toward the furrow cells. Apical width was measured as the distance between the apical-most contact points of the cell to its neighbors. Basal width was measured as the distance between the basal-most contact points between the cell and its neighbors, apical to the furrow canals or yolk stalks. Aspect ratio was defined as the ratio between width and height. Relative nuclear position was determined by dividing the distance of the nuclear center from the base of the cell by the height of the cell. Morphogenetic data were plotted showing the median, quartiles and highest and lowest data points. Morphometric data were compared using two-way ANOVA with a Tukey post-test. During late phase 2, edge cells and invaginated cells were compared to other cells using one-way ANOVA with a Tukey post-test, except for apical width to basal width ratios, which were compared using the Kruskal–Wallis test with Dunn's post-test. Arm intensity differences were compared using the Kruskal–Wallis test with Dunn's post-test. Phalloidin intensity differences between cell types and morphological phases were compared using two-way ANOVA with a Tukey post-test. Phalloidin intensity differences between invaginated cells and other cell types during late phase 2 were compared using one-way ANOVA with a Tukey post-test. Sqh-GFP intensity measurements were made on maximum intensity z-stack projections and were compared using either one-way ANOVA with a Tukey post-test for total apical myosin or by the Kruskal–Wallis test with Dunn's post-test for medioapical and subapical myosin.

References

Anderson, K.V., Jurgens, G., Nusslein-Volhard, C., 1985. Establishment of dorsal-ventral polarity in the *Drosophila* embryo: genetic studies on the role of the Toll gene product. Cell 42, 779–789.

Baum, B., Georgiou, M., 2011. Dynamics of adherens junctions in epithelial establishment, maintenance, and remodeling. J. Cell Biol. 192, 907–917.

Bertet, C., Sulak, L., Lecuit, T., 2004. Myosin-dependent junction remodelling controls planar cell intercalation and axis elongation. Nature 429, 667–671.

Blankenship, J.T., Backovic, S.T., Sanny, J.S., Weitz, O., Zallen, J.A., 2006. Multicellular rosette formation links planar cell polarity to tissue morphogenesis. Dev. Cell 11, 459–470.

Blankenship, J.T., Wieschaus, E., 2001. Two new roles for the *Drosophila* AP patterning system in early morphogenesis. Development 128, 5129–5138.

Campos-Ortega, J.A., Hartenstein, V., 1997. The Embryonic Development of *Drosophila Melanogaster*. Springer-Verlag, Berlin.

Cavey, M., Lecuit, T., 2008. Imaging cellular and molecular dynamics in live embryos using fluorescent proteins. Methods Mol. Biol. 420, 219–238.

Costa, M., Sweeton, D., Wieschaus, E., 1993. Gastrulation in *Drosophila*: cellular mechanisms of morphogenetic movements In: Bate, M., Martinez-Arias, A.

(Eds.), The Development of *Drosophila Melanogaster*. Cold Spring Harbor Press, Cold Spring Harbor.

Davidson, L.A., 2012. Epithelial machines that shape the embryo. Trends Cell Biol. 22, 82–87.

Davidson, L.A., Koehl, M.A., Keller, R., Oster, G.F., 1995. How do sea urchins invaginate? Using biomechanics to distinguish between mechanisms of primary invagination. Development 121, 2005–2018.

Davidson, L.A., Oster, G.F., Keller, R.E., Koehl, M.A., 1999. Measurements of mechanical properties of the blastula wall reveal which hypothesized mechanisms of primary invagination are physically plausible in the sea urchin *Strongylocentrotus purpuratus*. Dev. Biol 209, 221–238.

Dawes-Hoang, R.E., Parmar, K.M., Christiansen, A.E., Phelps, C.B., Brand, A.H., Wieschaus, E.F., 2005. Folded gastrulation, cell shape change and the control of myosin localization. Development 132, 4165–4178.

Driever, W., Nusslein-Volhard, C., 1988. The bicoid protein determines position in the *Drosophila* embryo in a concentration-dependent manner. Cell 54, 95–104.

Ettensohn, C.A., 1985. Mechanisms of epithelial invagination. Q. Rev. Biol. 60, 289–307.

Fehon, R.G., Dawson, I.A., Artavanis-Tsakonas, S., 1994. A *Drosophila* homologue of membrane-skeleton protein 4.1 is associated with septate junctions and is encoded by the coracle gene. Development 120, 545–557.

Foe, V.E., 1989. Mitotic domains reveal early commitment of cells in *Drosophila* embryos. Development 107, 1–22.

Fristrom, D., 1988. The cellular basis of epithelial morphogenesis. A review. Tissue Cell 20, 645–690.

Fritz, A.E., Ikmi, A., Seidel, C., Paulson, A., Gibson, M.C., 2013. Mechanisms of tentacle morphogenesis in the sea anemone *Nematostella vectensis*. Development 140, 2212–2223.

Frohnhofer, H.G., Nusslein-Volhard, C., 1986. Organization of anterior pattern in the *Drosophila* embryo by the maternal gene bicoid. Nature 324, 120–125.

Gelbart, M.A., He, B., Martin, A.C., Thiberge, S.Y., Wieschaus, E.F., Kaschube, M., 2012. Volume conservation principle involved in cell lengthening and nucleus movement during tissue morphogenesis. Proc. Natl. Acad. Sci. USA 109, 19298–19303.

Hardin, J., Keller, R., 1988. The behaviour and function of bottle cells during gastrulation of *Xenopus laevis*. Development 103, 211–230.

Harding, K., Rushlow, C., Doyle, H.J., Hoey, T., Levine, M., 1986. Cross-regulatory interactions among pair-rule genes in *Drosophila*. Science 233, 953–959.

Harris, T.J., Peifer, M., 2004. Adherens junction-dependent and -independent steps in the establishment of epithelial cell polarity in *Drosophila*. J. Cell Biol. 167, 135–147.

Harris, T.J., Peifer, M., 2005. The positioning and segregation of apical cues during epithelial polarity establishment in *Drosophila*. J. Cell Biol. 170, 813–823.

Harris, T.J., Tepass, U., 2010. Adherens junctions: from molecules to morphogenesis. Nat. Rev. Mol. Cell. Biol. 11, 502–514.

Herman, T., Hartwieg, E., Horvitz, H.R., 1999. sqv mutants of *Caenorhabditis elegans* are defective in vulval epithelial invagination. Proc. Natl. Acad. Sci. USA 96, 968–973.

Hohn, S., Hallmann, A., 2011. There is more than one way to turn a spherical cellular monolayer inside out: type B embryo inversion in *Volvox globator*. BMC Biol. 9, 89.

Ikebe, M., Hartshorne, D.J., 1985. Phosphorylation of smooth muscle myosin at two distinct sites by myosin light chain kinase. J. Biol. Chem. 260, 10027–10031.

Ikebe, M., Hartshorne, D.J., Elzinga, M., 1986. Identification, phosphorylation, and dephosphorylation of a second site for myosin light chain kinase on the 20,000-dalton light chain of smooth muscle myosin. J. Biol. Chem. 261, 36–39.

Ikebe, M., Koretz, J., Hartshorne, D.J., 1988. Effects of phosphorylation of light chain residues threonine 18 and serine 19 on the properties and conformation of smooth muscle myosin. J. Biol. Chem. 263, 6432–6437.

Irish, V.F., Gelbart, W.M., 1987. The decapentaplegic gene is required for dorsal-ventral patterning of the *Drosophila* embryo. Genes Dev. 1, 868–879.

Jacinto, A., Wood, W., Balayo, T., Turmaine, M., Martinez-Arias, A., Martin, P., 2000. Dynamic actin-based epithelial adhesion and cell matching during *Drosophila* dorsal closure. Curr. Biol. 10, 1420–1426.

Kam, Z., Minden, J.S., Agard, D.A., Sedat, J.W., Leptin, M., 1991. *Drosophila* gastrulation: analysis of cell shape changes in living embryos by three-dimensional fluorescence microscopy. Development 112, 365–370.

Keller, R., Davidson, L.A., Shook, D.R., 2003. How we are shaped: the biomechanics of gastrulation. Differentiation 71, 171–205.

Keller, R., Shook, D., 2011. The bending of cell sheets–from folding to rolling. BMC Biol. 9, 90.

Kiehart, D.P., Galbraith, C.G., Edwards, K.A., Rickoll, W.L., Montague, R.A., 2000. Multiple forces contribute to cell sheet morphogenesis for dorsal closure in Drosophila. J. Cell Biol. 149, 471–490.

Kondo, T., Hayashi, S., 2013. Mitotic cell rounding accelerates epithelial invagination. Nature 494, 125–129.

Kress, H., Stelzer, E.H., Holzer, D., Buss, F., Griffiths, G., Rohrbach, A., 2007. Filopodia act as phagocytic tentacles and pull with discrete steps and a load-dependent velocity. Proc. Natl. Acad. Sci. USA 104, 11633–11638.

Laprise, P., Tepass, U., 2011. Novel insights into epithelial polarity proteins in *Drosophila*. Trends Cell Biol. 21, 401–408.

Larsen, C.W., Hirst, E., Alexandre, C., Vincent, J.P., 2003. Segment boundary formation in *Drosophila* embryos. Development 130, 5625–5635.

Lecuit, T., Lenne, P.F., 2007. Cell surface mechanics and the control of cell shape, tissue patterns and morphogenesis. Nat. Rev. Mol. Cell. Biol. 8, 633–644.

Lecuit, T., Lenne, P.F., Munro, E., 2011. Force generation, transmission, and integration during cell and tissue morphogenesis. Annu. Rev. Cell Dev. Biol. 27, 157–184.

Lee, J.Y., Harland, R.M., 2007. Actomyosin contractility and microtubules drive apical constriction in *Xenopus* bottle cells. Dev. Biol. 311, 40–52.

Lehmann, R., Nusslein-Volhard, C., 1987. hunchback, a gene required for segmentation of an anterior and posterior region of the *Drosophila* embryo. Dev. Biol. 119, 402–417.

Leptin, M., Grunewald, B., 1990. Cell shape changes during gastrulation in *Drosophila*. Development 110, 73–84.

Llimargas, M., Casanova, J., 2010. Apical constriction and invagination: a very self-reliant couple. Dev. Biol. 344, 4–6.

Magie, C.R., Daly, M., Martindale, M.Q., 2007. Gastrulation in the cnidarian *Nematostella vectensis* occurs via invagination not ingression. Dev. Biol. 305, 483–497.

Mammoto, T., Ingber, D.E., 2010. Mechanical control of tissue and organ development. Development 137, 1407–1420.

Martin, A.C., Gelbart, M., Fernandez-Gonzalez, R., Kaschube, M., Wieschaus, E.F., 2010. Integration of contractile forces during tissue invagination. J. Cell Biol. 188, 735–749.

Martin, A.C., Goldstein, B., 2014. Apical constriction: themes and variations on a cellular mechanism driving morphogenesis. Development 141, 1987–1998.

Martin, A.C., Kaschube, M., Wieschaus, E.F., 2009. Pulsed contractions of an actin-myosin network drive apical constriction. Nature 457, 495–499.

McGill, M.A., McKinley, R.F., Harris, T.J., 2009. Independent cadherin-catenin and Bazooka clusters interact to assemble adherens junctions. J. Cell Biol. 185, 787–796.

Millard, T.H., Martin, P., 2008. Dynamic analysis of filopodial interactions during the zippering phase of *Drosophila* dorsal closure. Development 135, 621–626.

Morin, X., Daneman, R., Zavortink, M., Chia, W., 2001. A protein trap strategy to detect GFP-tagged proteins expressed from their endogenous loci in *Drosophila*. Proc. Natl. Acad. Sci. USA 98, 15050–15055.

Muller, H.A., Wieschaus, E., 1996. armadillo, bazooka, and stardust are critical for early stages in formation of the zonula adherens and maintenance of the polarized blastoderm epithelium in *Drosophila*. J. Cell Biol. 134, 149–163.

Namba, R., Pazdera, T.M., Cerrone, R.L., Minden, J.S., 1997. *Drosophila* embryonic pattern repair: how embryos respond to bicoid dosage alteration. Development 124, 1393–1403.

Nishimura, T., Honda, H., Takeichi, M., 2012. Planar cell polarity links axes of spatial dynamics in neural-tube closure. Cell 149, 1084–1097.

Nishimura, T., Takeichi, M., 2008. Shroom3-mediated recruitment of Rho kinases to the apical cell junctions regulates epithelial and neuroepithelial planar remodeling. Development 135, 1493–1502.

Oda, H., Tsukita, S., 2001. Real-time imaging of cell-cell adherens junctions reveals that *Drosophila* mesoderm invagination begins with two phases of apical constriction of cells. J. Cell Sci. 114, 493–501.

Odell, G.M., Oster, G., Alberch, P., Burnside, B., 1981. The mechanical basis of morphogenesis. I. Epithelial folding and invagination. Dev. Biol. 85, 446–462.

Payre, F., Crozatier, M., Vincent, A., 1994. Direct control of transcription of the *Drosophila* morphogen bicoid by the serendipity delta zinc finger protein, as revealed by in vivo analysis of a finger swap. Genes Dev. 8, 2718–2728.

Plageman Jr., T.F., Chung, M.I., Lou, M., Smith, A.N., Hildebrand, J.D., Wallingford, J.B., Lang, R.A., 2010. Pax6-dependent Shroom3 expression regulates apical constriction during lens placode invagination. Development 137, 405–415.

Pollard, T.D., Borisy, G.G., 2003. Cellular motility driven by assembly and disassembly of actin filaments. Cell 112, 453–465.

Quintin, S., Gally, C., Labouesse, M., 2008. Epithelial morphogenesis in embryos: asymmetries, motors and brakes. Trends Genet. 24, 221–230.

Rickoll, W.L., 1976. Cytoplasmic continuity between embryonic cells and the primitive yolk sac during early gastrulation in *Drosophila melanogaster*. Dev. Biol. 49, 304–310.

Rickoll, W.L., Counce, S.J., 1980. Morphogenesis of the embryo of *Drosophila melanogaster* - germ band extension. Wilhelm Roux's Arch. Dev. Biol. 188, 163–177.

Rodriguez-Mesa, E., Abreu-Blanco, M.T., Rosales-Nieves, A.E., Parkhurst, S.M., 2012. Developmental expression of *Drosophila* Wiskott-Aldrich Syndrome family proteins. Dev. Dyn. 241, 608–626.

Roth, S., Hiromi, Y., Godt, D., Nusslein-Volhard, C., 1991. Cactus, a maternal gene required for proper formation of the dorsoventral morphogen gradient in *Drosophila* embryos. Development 112, 371–388.

Royou, A., Sullivan, W., Karess, R., 2002. Cortical recruitment of nonmuscle myosin II in early syncytial *Drosophila* embryos: its role in nuclear axial expansion and its regulation by Cdc2 activity. J. Cell Biol. 158, 127–137.

Rushlow, C., Levine, M., 1990. Role of the zerknullt gene in dorsal-ventral pattern formation in *Drosophila*. Adv. Genet. 27, 277–307.

Sawyer, J.K., Harris, N.J., Slep, K.C., Gaul, U., Peifer, M., 2009. The *Drosophila* afadin homologue Canoe regulates linkage of the actin cytoskeleton to adherens junctions during apical constriction. J. Cell Biol. 186, 57–73.

Sawyer, J.M., Harrell, J.R., Shemer, G., Sullivan-Brown, J., Roh-Johnson, M., Goldstein, B., 2010. Apical constriction: a cell shape change that can drive morphogenesis. Dev. Biol. 341, 5–19.

Schupbach, T., Wieschaus, E., 1986. Maternal-effect mutations altering the anterior-posterior pattern of the *Drosophila* embryo. Roux's Arch. Dev. Biol. 195, 302–317.

Schupbach, T., Wieschaus, E., 1989. Female sterile mutations on the second chromosome of *Drosophila melanogaster*. I. Maternal effect mutations. Genetics 121, 101–117.

Sherrard, K., Robin, F., Lemaire, P., Munro, E., 2010. Sequential activation of apical and basolateral contractility drives ascidian endoderm invagination. Curr. Biol. 20, 1499–1510.

Simoes, S., Denholm, B., Azevedo, D., Sotillos, S., Martin, P., Skaer, H., Hombria, J.C., Jacinto, A., 2006. Compartmentalisation of Rho regulators directs cell invagination during tissue morphogenesis. Development 133, 4257–4267.

Sokac, A.M., Wieschaus, E., 2008. Local actin-dependent endocytosis is zygotically controlled to initiate Drosophila cellularization. Dev. Cell 14, 775–786.

Spahn, P., Ott, A., Reuter, R., 2012. The PDZ-GEF protein Dizzy regulates the establishment of adherens junctions required for ventral furrow formation in Drosophila. J. Cell Sci. 125, 3801–3812.

St Pierre, S.E., Ponting, L., Stefancsik, R., McQuilton, P., 2014. FlyBase 102–advanced approaches to interrogating FlyBase. Nucleic Acids Res. 42, D780–D788.

Struhl, G., Struhl, K., Macdonald, P.M., 1989. The gradient morphogen bicoid is a concentration-dependent transcriptional activator. Cell 57, 1259–1273.

Sweeton, D., Parks, S., Costa, M., Wieschaus, E., 1991. Gastrulation in Drosophila: the formation of the ventral furrow and posterior midgut invaginations. Development 112, 775–789.

Tepass, U., Hartenstein, V., 1994. The development of cellular junctions in the Drosophila embryo. Dev. Biol. 161, 563–596.

Thomas, J.H., Wieschaus, E., 2004. src64 and tec29 are required for microfilament contraction during Drosophila cellularization. Development 131, 863–871.

Turner, F.R., Mahowald, A.P., 1977. Scanning electron microscopy of Drosophila melanogaster embryogenesis. II. Gastrulation and segmentation. Dev. Biol. 57, 403–416.

Underwood, E.M., Turner, F.R., Mahowald, A.P., 1980. Analysis of cell movements and fate mapping during early embryogenesis in Drosophila melanogaster. Dev. Biol. 74, 286–301.

Viamontes, G.I., Kirk, D.L., 1977. Cell shape changes and the mechanism of inversion in Volvox. J. Cell Biol. 75, 719–730.

Vincent, A., Blankenship, J.T., Wieschaus, E., 1997. Integration of the head and trunk segmentation systems controls cephalic furrow formation in Drosophila. Development 124, 3747–3754.

Wang, Y.C., Khan, Z., Kaschube, M., Wieschaus, E.F., 2012. Differential positioning of adherens junctions is associated with initiation of epithelial folding. Nature 484, 390–393.

Wang, Y.C., Khan, Z., Wieschaus, E.F., 2013. Distinct Rap1 activity states control the extent of epithelial invagination via alpha-catenin. Dev. Cell 25, 299–309.

Wieschaus, E., Nüsslein-Volhard, C., 1998. Looking at embryos In: Roberts, D.B. (Ed.), Drosophila: A Practical Approach, 2nd ed. Oxford University Press, Oxford, pp. 179–214.

Wodarz, A., Ramrath, A., Kuchinke, U., Knust, E., 1999. Bazooka provides an apical cue for Inscuteable localization in Drosophila neuroblasts. Nature 402, 544–547.

Young, P.E., Pesacreta, T.C., Kiehart, D.P., 1991. Dynamic changes in the distribution of cytoplasmic myosin during Drosophila embryogenesis. Development 111, 1–14.

Zallen, J.A., Wieschaus, E., 2004. Patterned gene expression directs bipolar planar polarity in Drosophila. Dev. Cell 6, 343–355.

Zhang, L., Ward, R.E., 2011. Distinct tissue distributions and subcellular localizations of differently phosphorylated forms of the myosin regulatory light chain in Drosophila. Gene Expr. Patterns 11, 93–104.

Zhang, Y., Kong, D., Reichl, L., Vogt, N., Wolf, F., Grosshans, J., 2014. The glucosyltransferase Xiantuan of the endoplasmic reticulum specifically affects E-Cadherin expression and is required for gastrulation movements in Drosophila. Dev. Biol. 390, 208–220.

Zusman, S.B., Sweeton, D., Wieschaus, E.F., 1988. short gastrulation, a mutation causing delays in stage-specific cell shape changes during gastrulation in Drosophila melanogaster. Dev. Biol. 129, 417–427.

Zusman, S.B., Wieschaus, E.F., 1985. Requirements for zygotic gene activity during gastrulation in Drosophila melanogaster. Dev. Biol. 111, 359–371.